Master's thesis

NTNU
Norwegian University of Science and Technology
Faculty of Natural Sciences
Department of Biotechnology and Food Science

Asle Hammer Berget

Using carbohydrates to improve a hypothetical process for the enzymatic degradation of PET

Master's thesis in MBIOT5
Supervisor: Gaston Courtade
Co-supervisor: Finn Lillelund Aachmann
May 2023

NTNU
Norwegian University of
Science and Technology

Asle Hammer Berget

Using carbohydrates to improve a hypothetical process for the enzymatic degradation of PET

Master's thesis in MBIOT5
Supervisor: Gaston Courtade
Co-supervisor: Finn Lillelund Aachmann
May 2023

Norwegian University of Science and Technology
Faculty of Natural Sciences
Department of Biotechnology and Food Science

NTNU
Norwegian University of
Science and Technology

Abstract

Plastics have been established as excellent materials for numerous applications. Many plastics are tough, lightweight, cheap, and have barrier properties. The ubiquitous presence of plastics, along with insufficient disposal methods have led to the accumulation of plastics in the environment, especially threatening marine ecosystems. In addition, most plastics are made from non-sustainable petrochemical sources, and because of this, recycling is a necessary process.

Poly (ethylene terephthalate) (PET) is a polyester plastic found in beverage containers, packaging, and clothing. Today, only clear, clean PET is recycled in mostly thermomechanical ways, which is associated with a quality loss for each cycle. This downcycling of the non-sustainably produced PET is a problem that needs solving.

In this master's thesis, a hypothetical enzymatic degradation process was envisioned, where end-of-life PET is degraded to its monomers, and resynthesized to have the same quality as virgin PET. The overarching aim of the thesis was to use carbohydrates to improve this process.

An open loop process was suggested, where part of the stream of degradation products can be used to synthesize more valuable products in an upcycling manner. The upcycling explored in this thesis was to use carbohydrates, specifically glucans, and terephthalic acid (TPA), one of the monomers of PET to make a novel material with potentially interesting properties for various applications.

The cellulose terephthalate (CTP) ester hypothesized in the thesis could have some interesting properties that make it an attractive polymer, for example film forming capabilities. In addition, a β-cyclodextrin terephthalate ester was envisioned, where the terephthalate residue could perhaps introduce pH tuned complexation.

Glucose and cellopentaose were used as model carbohydrates to gain insight on the feasibility of the desired reaction, where *p*-Toluenesulfonyl chloride (TsCl) was used as an activator of the primary hydroxyl group in the glucans, and as an in situ activator of TPA. No clear evidence of terephthalation was seen for glucose, cellopentaose, cellulose, or β-cyclodextrin (CD) using NMR spectroscopy and FTIR spectroscopy. Despite this, the existence of the glucan terephthalate esters were not disproved, and further efforts should be made to enable upcycling of PET degradation products, possibly by using carbohydrates.

One of the bottlenecks of enzymatic degradation of PET is low rate, which was addressed by using the carbohydrate group cyclodextrins (CDs). Complexation of α-CD and β-CD with TPA was determined before the effect of the cyclodextrins on the degradation rate of a PET hydrolyzing enzyme, *Fusarium solani pisi* cutinase (FsC), was investigated. The enzymatic degradation of PET was monitored with time-resolved ^{1}H-NMR.

Apparent degradation rates for the main degradation product, MHET, was doubled with either of the CDs present. Another finding was that the two cyclodextrins affected the product distribution differently. Presence of the smaller α-CD gave higher concentration than the control experiment for the smallest of the aromatic degradation products, TPA. The larger β-CD's presence favored the production of larger degradation products, and had the highest concentration of BHET of the three experiments. In addition, unidentified ^{1}H-NMR peaks were observed when β-CD was present at 8.05 to 8.13 ppm, and could possibly originate from soluble PET oligomers.

The results presented in this thesis may not contribute significantly towards the public introduction of enzymatic recycling of PET. Nevertheless, this thesis explored some basic ideas for the utilization of carbohydrates to promote upcycling of plastic waste degradation products, and by reducing product inhibition for the FsC for the overall improvement of a hypothetical enzymatic degradation of PET process.

Sammendrag

Plast har blitt etablert som utmerkede materialer med mange bruksområder. Mange plasttyper er hardføre, lette, billige og har barriereegenskaper. Den utbredte tilstedeværelsen av plast, sammen med utilstrekkelige avfallsbehandlingsmetoder, har ført til opphopning av plast i miljøet, noe som kan true spesielt marine økosystemer. I tillegg er de fleste plasttyper laget fra ikke-bærekraftige petrokjemiske kilder, derfor er gjenvinning av plast en nødvendig prosess.

Poly (etylentereftalat) (PET) er en polyesterplast som finnes i drikkeflasker, emballasje, og klær. I dag blir bare gjennomsiktig, ren PET resirkulert på hovedsakelig termomekaniske måter, noe som er assosiert med et kvalitetstap for hver syklus. Denne «nedsirkuleringen» av ikke-bærekraftig produsert PET er et problem som må løses.

I denne masteroppgaven ble det konseptualisert en hypotetisk enzymatisk nedbrytningsprosess der PET-avfall brytes ned til monomerene sine og resyntetiseres for å ha samme kvalitet som såkalt jomfru-PET. Det overordnede målet med oppgaven var å bruke karbohydrater for å forbedre denne prosessen.

En åpen syklus-prosess ble foreslått, der en del av strømmen av nedbrytningsprodukter kan brukes til å syntetisere mer verdifulle produkter enn ny PET, såkalt «oppsirkulering». Oppsirkuleringen som ble undersøkt i denne oppgaven var å bruke karbohydrater, spesielt glukaner og tereftalsyre (TPA), en av monomerene i PET, for å lage et nytt materiale med potensielt interessante egenskaper for ulike applikasjoner.

Glukose og cellopentaose ble brukt som modellkarbohydrater for å få innsikt i gjennomførbarheten av den ønskede reaksjonen, der *p*-Toluenesulfonylklorid (TsCl) ble brukt som en aktivator av den primære hydroksylgruppen i glukanene, og som en in situ-aktivator av TPA. Ingen klare bevis på tereftalering ble sett for glukose, cellopentaose, cellulose eller β-syklodekstrin ved bruk av NMR-spektroskopi og FTIR-spektroskopi. Til tross for dette ble ikke eksistensen av glukan-tereftalatesterene motbevist, og ytterligere innsats bør gjøres for å muliggjøre oppsirkulering av PET-nedbrytningsprodukter, muligens ved å bruke karbohydrater.

En av flaskehalsene ved enzymatisk nedbrytning av PET er lav hastighet, som ble adressert i denne oppgaven ved å bruke karbohydratgruppen syklodekstriner. Inklusjonskompleksdannelse av α- og β-syklodekstrin med TPA ble bestemt, før effekten av syklodekstrinene på nedbrytningshastigheten til et PET-hydrolyserende enzym, *Fusarium solani pisi* cutinase (FsC), ble undersøkt. Den enzymatiske nedbrytningen av PET ble overvåket med tidsoppløst ^{1}H-NMR.

Tilsynelatende nedbrytningshastigheter for hovednedbrytningsproduktet, MHET, ble doblet med syklodekstrinene til stede. De to ulike syklodekstrinene påvirket nedbrytningen av PET forskjellig, noe som resulterte i forskjellige produktfordelinger. Tilstedeværelsen av den mindre α-syklodekstrin ga høyere konsentrasjon enn kontrolleksperimentet for det minste av de aromatiske nedbrytningsproduktene, TPA. Den større β-syklodekstrins tilstedeværelse fremmet produksjonen av større nedbrytningsprodukter og hadde høyest konsentrasjon av BHET av de tre eksperimentene. I tillegg ble uidentifiserte ^{1}H-NMR-signaler observert da β-syklodekstrin var til stede ved 8,05 til 8,13 ppm og kan muligens stamme fra løselige PET-oligomerer.

Resultatene presentert i denne oppgaven kan kanskje ikke bidra vesentlig til den offentlige introduksjonen av enzymatisk resirkulering av PET. Likevel ble noen grunnleggende ideer utforsket i denne oppgaven når det gjelder utnyttelse av karbohydrater for å fremme oppsirkulering av plastavfall-snedbrytningsprodukter, og for å redusere produktinhibering for FsC for den generelle forbedringen av en hypotetisk enzymatisk PET-nedbrytningprosess.

Preface

The work done in this master's thesis was carried out at the Department of Biotechnology and Food Science at the Faculty of Natural Sciences at the Norwegian University of Science and Technology (NTNU) between August 2022 and May 2023.

For my supervisor, Gaston Courtade, I would like to express deep gratitude for ideas, discussions, support, criticism, inspiration, independence, and trust. Your enthusiasm is unparalleled. Thank you for providing the opportunity to learn much about the the plastic problem and potential solutions, and guidance along the way. It has been a privilege to be a part of your team. Thank you to the other members of the team as well: Davide, Kristoffer, Susanne, and Tina, for advice and help throughout my master's project. Thank you to my co-supervisor Finn Lillelund Aachmann for important insight and resources.

To the Biopolymers and Biomaterials group at NTNU, thank you for interesting presentations and social meetings.

Finally, thank you to all my fellow master students, friends and co-habitants, and family who have supported me during this special year, thank you for love and laughter.

Trondheim, May 15th, 2023
Asle Hammer Berget

Contents

List of Figures

List of Tables

List of symbols and abbreviations

α-CD	α-Cyclodextrin
β-CD	β-Cyclodextrin
γ-CD	γ-Cyclodextrin
δ^1H	Chemical shift of protons
$\Delta\delta^1$H	Change in chemical shift of protons
$\Delta\delta^1H_{max}$	Maximum change in chemical shift of cyclodextrin protons at saturation of guest molecules
$\Delta\delta^1H_{obs}$	Observed change in chemical shift of cyclodextrin protons
AGU	Anhydroglucose unit
BHET	Bis-(2-hydroxyethyl) terephthalate
BMIMCl	1-butyl-3-methylimidazolium chloride
BMIMOAc	1-butyl-3-methylimidazolium acetate
CD	Cyclodextrin
[CD]	Concentration of cyclodextrin
CTP	Cellulose terephthalate
D	Diffusion coefficient
DMSO-d_6	Dimethyl sulfoxide-d_6
DOSY	Diffusion Ordered Spectroscopy
EG	Ethylene glycol
FsC	*Fusarium solani pisi* Cutinase
FTIR	Fourier Transform Infrared (spectroscopy)
G	Guest molecule
[G]	Concentration of guest molecule
^{1}H	Protium
HMBC	Heteronuclear Multiple Bond Correlation spectroscopy
HSQC	Heteronuclear Single-Quantum Correlation spectroscopy
K_a	Association constant
K_d	Dissociation constant
MHET	Mono-(2-hydroxyethyl) terephthalate
NMR	Nuclear Magnetic Resonance (spectroscopy)
OD_{600}	Optical density at 600 nm
PET	Poly (ethylene terephthalate)
ppm	Parts per million
TOSC	Tosylated cellulose
TPA	Terephthalic acid
TsCl	*p*-Toluenesulfonyl chloride
TsOH	*p*-Toluenesulfonic acid
UV	Ultraviolet

1 Background and Introduction

1.1 The Plastic Problem

Plastics have been established as excellent industrial, biomedical, and packaging materials. The nuances of plastic composition, additives and structure give rise to subtle differences in applications for different kinds of plastics. Many plastics are tough, lightweight, malleable, and have barrier properties. This has led to the ubiquitous presence of these synthetic materials in society and the environment. Yearly production of plastics from petrochemical sources has increased for many years, while recycling methods remain inadequate to safely dispose the increasing amounts of plastics produced. Accumulation of non-biodegradable plastics has therefore become a recognized threat to the environment, and solving the problem is long overdue (Ilyas et al. (2018)).

1.1.1 Marine Organisms are Threatened by Runaway Plastic Waste

Because of its toughness and resistance to degradation, runaway plastic waste persist in the environment. Coming from mainly consumer products, industry, and fishing, much of the land-based plastics end up in oceans through rivers and wastewater treatment plants, at higher concentrations near densely populated areas (Li et al. (2016)).

Macro- (larger than 25 mm), micro- (100 nm-25 mm), and nano-plastics (smaller than 100 nm) can all be harmful to marine organisms. Plastics in the ocean are exposed to erosive processes, continually reducing their size, from large pieces, to smaller fragments, all the way down to particles. Fragmentation can occur physically, chemically, and biologically, for example mechanical weathering, photodegradation from sunlight, and chemical oxidation, leading to microbial degradation when fragments reach sufficiently small size and oxidized state (Li et al. (2016)). Because these factors are all present on beaches, they are the environmental sites with the highest rates of plastic degradation (Corcoran et al. (2009)).

Ingestion of plastics can lead to gastrointestinal blockage, enzyme secretion inhibition, loss of appetite, and reproductive failure. Plastics can also carry bioaccumulating compounds into marine organisms, and plastic additives can cause endocrine disruption (Li et al. (2016)). Entanglement can be lethal and restrict the animal's ability to hunt or escape predators. Macroplastics, such as packing loops and fishing equipment, are the primary causes of entanglement (Li et al. (2016)).

1.2 Recycling of PET-Plastic

1.2.1 PET-Plastic

One of the most common consumer plastics is poly(ethylene terephthalate) (PET), found in beverage bottles, single-use packaging and polyester clothes. PET is a polyester made of terephthalic acid (TPA) and ethylene glycol (EG), as shown in Figure 1. Synthesis of PET happens in two steps, esterification of TPA and EG, and subsequent polycondensation. The repeating chemical structure of PET is shown in Figure 1, along with its monomers and degradation products. TPA provides rigidity, while EG gives flexibility to the polymer chains. The aromatic and planar nature of TPA gives rise to the high tensile strength through aromatic stacking of PET polymer chains. The strong intermolecular association is also the reason for the crystalline structure found in different kinds of PET (Long and Scheirs (2005)).

The crystalline structure of PET reduces access of water to individual chains, making the material insoluble and resistant to hydrolysis, one of the main mechanisms of biological and chemical degradation.

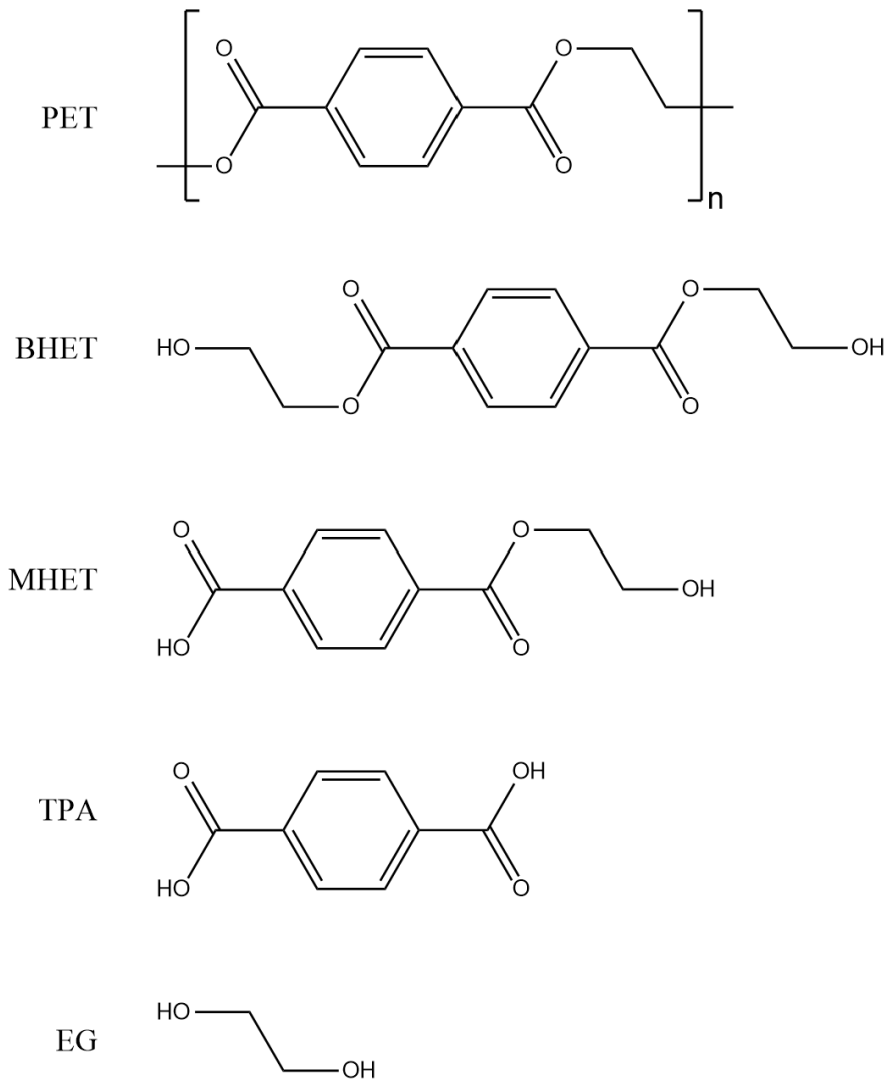

Figure 1: Chemical structure of PET and degradation products. BHET: Bis-(2-hydroxyethyl) terephthalate, MHET: Mono-(2-hydroxyethyl) terephthalate, TPA: Terephthalic acid, EG: Ethylene glycol.

1.2.2 Current recycling methods

In a European Union (EU) initiative from 2022 regarding the EU Strategy for Sustainable and Circular Textiles, it is encouraged to extend the lifespan of textiles, and improve collection of them at their end-of-life (European Commission (2022)). Convenient and cheap repair-services, and design in accordance to circularity are the primary ways to reduce waste, still acknowledging that textile apparel have to be discarded eventually. Along with other PET waste, polyester textiles need to be handled at their end-of-life.

Current disposal methods for PET bottles and containers include recycling, incineration, and landfill. Recycling is the most sustainable, long-term response to the problem, and can be done in different ways.

Thermomechanical recycling of PET is the most wide-spread and low-tech method, that provides granulates of mixed plastic, which are then extruded again to the desired products. The process leads to a decrease in quality of the material for each cycle, as it loses most of its toughness after only two cycles (López et al. (2014)). With this method, much of the food-grade PET can end up as insulation, shampoo bottles or flower pots (Vollmer et al. (2020)). This downcycling

limits the viability of thermomechanical recycling of PET as a sustainable solution to the plastic problem, because the synthesis of food-grade plastics require continuous input of virgin PET from non-renewable petroleum sources.

There are many ways to degrade PET chemically, and there have been advances in pyrolysis, alcoholysis, aminolysis, ammonolysis, neutral, acid, and alkali hydrolysis, and glycolysis (Thiounn and Smith (2020), Shojaei et al. (2020)).

Pyrolysis occurs at 450 ℃, and leads to many different side products, alcoholysis is done at 2-4 MPa and 180-280 ℃with toxic methanol in the process, aminolysis produce toxic amines, ammonolysis produce ammonium at more than 2 MPa and 70-180 ℃. Neutral hydrolysis rely on 1-4 MPa and 200-300 ℃, alkaline hydrolysis have around the same conditions, but strong alkali in addition, which can be toxic and corrosive, while acid hydrolysis has milder physical conditions, but strong acids can also be corrosive and toxic. Glycolysis is often dependent on catalysts to speed up the reaction, and the non-renewable zinc acetate salt is the most commonly used catalyst (Shojaei et al. (2020)).

Another, and perhaps more sophisticated method of recycling PET, is by using enzymes to degrade it to monomers. The wild-type bacteria *Ideonella sakaiensis* has been found to degrade and assimilate PET by evolution of the enzymes PETase and MHETase, however, reaction rates are currently too slow to be exploited for recycling applications (Yoshida et al. (2016)).

The main challenge with enzymatic recycling is the low reaction rates of PET degrading enzymes, and many efforts are being made to overcome the challenge. Targeted attempts at engineering more efficient PET-degrading enzymes have shown increase in degradation rate (Tournier et al. (2020)). Still, the commercialization of enzymatic depolymerization and recycling of PET is in its starting phase. An example is the patented Carbios process, that successfully utilizes engineered hydrolase enzymes from *Thermobifida alba* and *Fusarium solani pisi*, depending on the polyester (Thiounn and Smith (2020)). These reactions usually take place between 40 and 80 ℃, which brings a much lower energy cost than for many of the chemical polyester degradation processes (Vollmer et al. (2020)).

The enzymatic approach to degrading PET may be especially suited for textiles made of material blends, such as polyester and cotton, which is common in outdoors- and exercise clothing (Piribauer and Bartl (2019)). Polyester and cotton blends would require cumbersome separation before recycling, but owing to the specificity of enzymes and mild conditions, the polyester fibers could be degraded without affecting the cotton.

The potential of enzymatic recycling should continue to be explored. Illustrated in Figure 2 is an idealized process for recycling PET enzymatically in an open loop process. As PET products come to their end-of-life, illustrated by empty bottles, the waste is collected and sorted, then ground up to increase the surface area. This is part of what makes the process idealized, because in a real process, there is leakage to the environment. Also, different plastic blends may be impossible to separate, and will be downcycled. After preprocessing enzymatic degradation of PET commences, with the initial bottleneck being enzyme binding to insoluble PET surfaces. The second bottleneck is degradation time, which can be prolonged by degradation products remaining in the reaction vessel, occupying the enzymes. Recovery of the enzymes is another important factor for the viability of enzymatic recycling, as enzymes are expensive to produce. As PET is degraded, the monomers are preferentially removed from the reaction, and this stream can be split depending on the fate of the monomers. If synthesis of recycled PET is the objective, all degradation products are thought to be reacted together. If upcycling is the objective, separation of one of the monomers may be necessary. Upcycling part of the waste stream can open the loop and allow sustainable production of new biomaterials or biotechnological products.

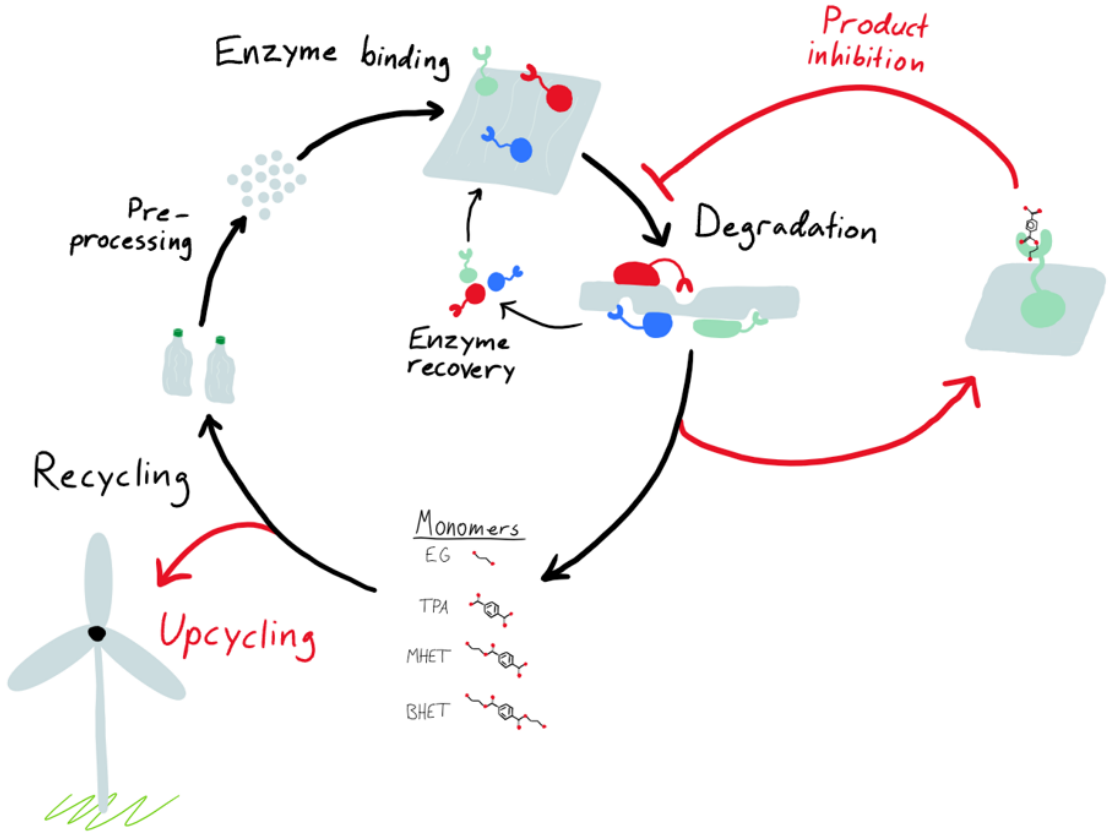

Figure 2: Overview of hypothetical process for enzymatic degradation of PET plastic. Marked in red are processes investigated in this thesis, upcycling and product inhibition. EG: Ethylene glycol, TPA: Terephthalic acid, MHET: Mono-(2-hydroxyethyl) terephthalate, BHET: Bis-(2-hydroxyethyl) terephthalate.

While plastics in the environment continue to be a problem onwards, and recycling methods and waste collection are not sufficiently developed, many attempts are being made to enable more sustainable recycling of plastics by combining different biotechnologies. This thesis was based on the idealized enzymatic recycling process described in Figure 2, and the aims are defined in section 2.

1.3 Carbohydrates to Improve Enzymatic Degradation of PET

Carbohydrates were explored as means of improving enzymatic degradation of PET. In this master's project, efforts were limited to upcycling of terephthalic acid and reduction of product inhibition during a degradation-reaction using a *F. solani* cutinase (FsC). The focus areas are highlighted in figure 2, which shows an overview of a hypothetical enzymatic degradation of PET process.

1.3.1 Upcycling of Terephthalic Acid Using Carbohydrates

An open-loop upcycling strategy may be a good option to incentivize enzymatic degradation of PET. Instead of synthesizing virgin PET, that will continue as single-use packaging, from degradation products, TPA can be funneled into a different process to make a high-value product. This valorization can justify resources spent on collecting waste, leading to an overall economically favorable process (Wei et al. (2020)).

1.3.2 Cellulose Terephthalate ester

In this master's project it was hypothesized that esterification of cellulose with TPA could be a possible way to upcycle PET hydrolysis products. As a justification for this hypotehesis textile waste was considered. In this context, material blends in textiles, such as polyester and cotton, which is common in outdoors- and exercise clothing, poses a recycling challenge (Piribauer and Bartl (2019)). A possible solution could be a chemoenzymatic process that uses enzymes to depolymerize polyester followed by chemical synthesis of a substituted cellulose with the reaction products. This would facilitate re- or upcycling of mixed fibers.

Semi-synthetic cellulose-based compounds have biomedical applications, from smaller substituents like sulfate and phosphate, to esters of carboxylic acids containing ammonium. Applications of these include tissue engineering, anticoagulation, antibacterial properties for wound dressings, drug delivery, and immobilization of bioactive compounds or enzymes (Yang et al. (2021))

In the hypothetical molecule "Cellulose Terephthalate" (CTP) (Figure 3), with sufficient degree of substitution, the crystalline structure would be less prominent than for pure cellulose. The CTP ester could also possibly be soluble, maybe contributing as a thickening and/or gelling agent, or even a plastic additive. There are many examples of the general applicability of cellulose esters to different products today. The commercially most important one, cellulose acetate is used for films, textiles, and coatings, and the properties are somewhat tunable by the degree of substitution. The properties of cellulose acetate butyrate can also be tuned by different compositions, and is used as a binder in coatings. Cellulose nitrate forms films, as well as being used as an explosive (Heinze et al. (2006)). Maybe the charge of TPA can resemble the nitrate group in cellulose nitrate, giving properties suitable for film forming for CTP, or provide hydrophobicity, similar to cellulose acetate butyrate.

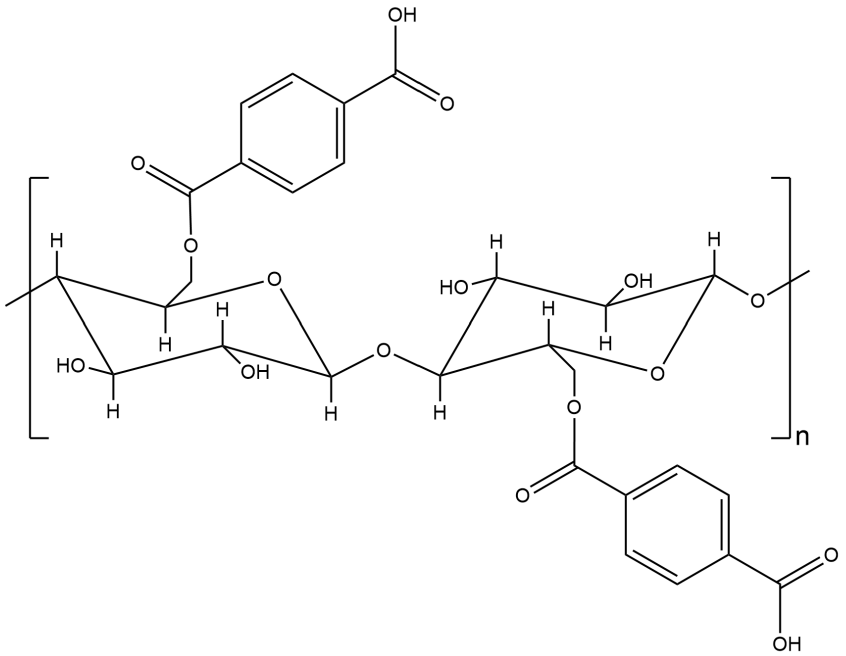

Figure 3: The hypothetical molecule "Cellulose Terephthalate", shown with degree of substitution = 1 per anhydroglucose unit (AGU). Maximum substitution for cellulose is 3 per AGU.

It is not only the properties of CTP itself that can seem alluring, as the possible context of processing an actual waste-stream directly through degradation and upcycling with all components present also seems ideal.

In a biochemical textile recycling process for material blends, the individual components are recovered, respun to fibers, and remade to fabric.

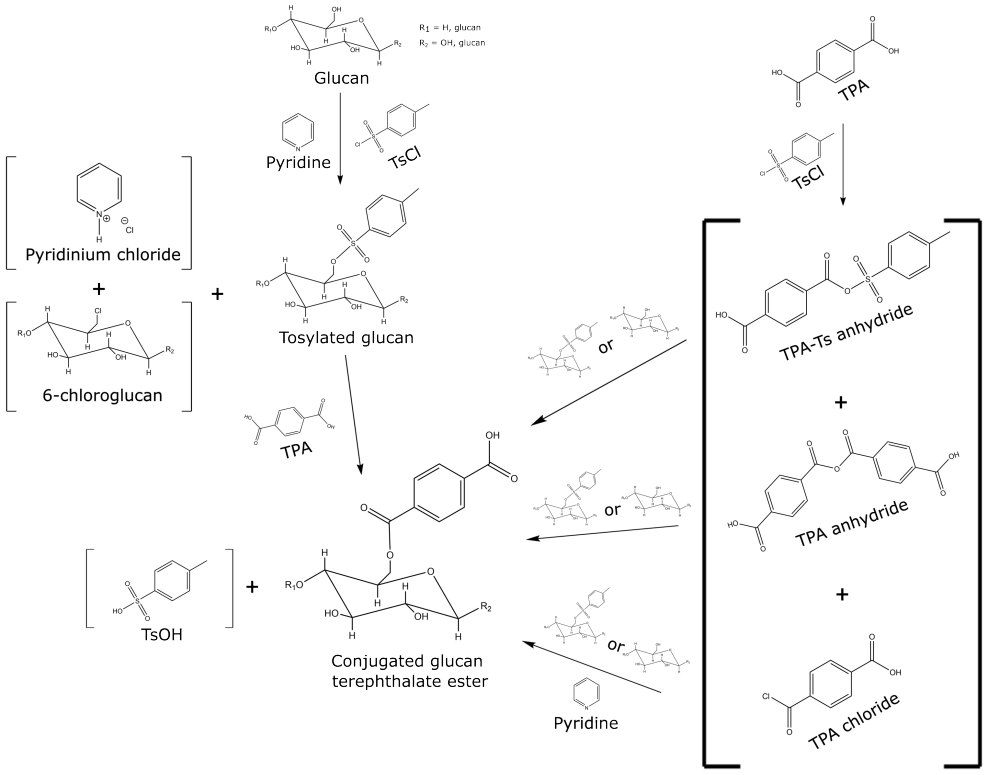

Figure 4: Possible reaction paths for the synthesis of a conjugated glucan terephthalate ester. Path I is attachment of a tosyl group which functions as a leaving group in a nucleophilic substitution. Path II is activation of the TPA by reaction with TsCl, forming a reactive mixture of mixed anhydride, terephthalic acid anhydride, and a terephthalic acid chloride that can conjugate the terephthalate residue to the glucan. Side products pyridinium chloride, chlorinated glucan, and TsOH are included.

Synthesis of cellulose esters presents two main challenges: poor cellulose solubility and activation. The first challenge can be addressed, for example, by using ionic liquids to dissolve cellulose (Gericke et al. (2012)). The second challenge depends on the nature of the reaction. In this master's thesis, based on previous research (Lease et al. (2021), Heinze et al. (2006)), the idea was to prime the C6 hydroxyl group for reaction by using *p*-toluenesulfonyl chloride (TsCl) as a leaving group, and also increase the reactivity of TPA by reaction with TsCl (Heinze et al. (2006)).

For the synthesis of CTP, a reaction scheme with two paths is suggested in Figure 4. Path I is based on using TsCl as a leaving group (Solomons and Fryhle (2007)), and Path II, the activation of TPA by TsCl (Heinze et al. (2006)).

1.3.3 Cyclodextrin-Terephthalate: Conjugation and Complexation

Expanding on the concept of cellulose terephthalate synthesis, this section delves into the potential of cyclodextrins, a versatile class of carbohydrates, as alternative candidates for TPA conjugation. Two key ideas are adressed in this context: first, the notion of covalently coupling terephthalic acid (TPA) to cyclodextrins to create novel cyclodextrin-TPA conjugates; and second, the interactions that might emerge between host-guest complex between cyclodextrins and TPA. The two key ideas address the highlighted aspects of an idealized enzymatic recycling process shown in Figure 2, upcycling, and product inhibition, which is explained in section 1.3.4.

Cyclodextrins (CDs) are cyclic oligosaccharides consisting of only α1,4 linked D-glucopyranoside monomers. The number of monomers is highly influential on their properties and applications, and the most common cyclodextrins are α-, β-, and γ-CDs, consisting of 6, 7 and 8 monomers,

respectively. Increasing the number of monomers leads to larger and less rigid cyclic molecules. Most properties, like increase in cavity diameter and volume, and decrease in pK_a, change smoothly with increasing size of cyclodextrins, except for water solubility. The even-numbered α- and γ-CD are much more water-soluble than β-CD (Steed and Atwood (2000)).

CDs are commonly represented as truncated cones that are hollow all the way through. Other molecules bind to the inside of the CD, forming an inclusion complex. One of the rims is wider than the other, where secondary hydroxyl groups of C2 and C3 face outward, while the narrower rim has primary hydroxyl groups of C6 facing outward (Steed and Atwood (2000)). The numbering of atoms in cyclodextrins is shown in figure 5, where, hydrogens 3, 5, and 6 are shown to protrude into the hollow cone-shape.

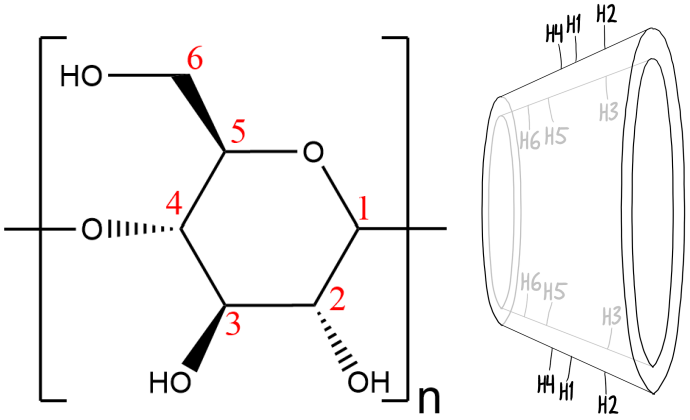

Figure 5: Left: Diagram of the monomer unit of cyclodextrins. Numbering of atoms in cyclodextrins follow the common numbering of a single glucose moiety. n=6 is α-, n=7 is β-, and n=8 is γ-cyclodextrin. Each type of cyclodextrin has n equivalent atoms of the same number. Right: General sketch of the shape of cyclodextrins, with relative positions of hydrogens on the toroidal shape indicated.

Complexation of cyclodextrins (CD) with non-polar guest molecules (G) is thought of as an equilibrium between bound (CD:G) and unbound states (equation 1). From this, the association constant (K_a) for the system can be defined as in equation 2, where K_d is the dissociation constant, and brackets signifies concentrations (Steed and Atwood (2000)).

$$CD + G \rightleftharpoons CD : G \tag{1}$$

$$K_a = \frac{[CD : G]}{[CD][G]} = \frac{1}{K_d} \tag{2}$$

NMR (Described in section 1.4.1) can be used to determine the association constant between cyclodextrins and a guest molecule (Schneider et al. (1998)). Here, it is assumed that a change in chemical shift ($\Delta\delta^1 H$) is directly related to the population differences of bound and unbound guest-molecules between two states. The two-state exchange model shown in equation 3 shows asymptotic behavior at high concentrations of guest molecule.

$$\Delta\delta^1 H_{obs} = \Delta\delta^1 H_{max} \times \frac{[CD] + [G] + K_d - \sqrt{([CD] + [G] + K_d)^2 - 4 \times [CD] \times [G]}}{2 \times [CD]} \tag{3}$$

where $\Delta\delta^1 H_{obs}$ is the observed chemical shift perturbation of CD protons caused by increasing concentrtaion of guest molecule ([G]), $\Delta\delta^1 H_{max}$ is the theoretical chemical shift perturbation when CD is saturated by guest molecules, [CD] is the concentration of cyclodextrin, and K_d is the dissociation constant for the inclusion complex CD:G.

Because of the complexation capability, cheap price, stability, non-toxicity, and decomplexation kinetics, CDs are widely used industrially. In the food industry, CDs can form complexes with expensive flavour oils and spices to reduce required amounts for the same flavour strength. CDs also stabilize pigments, which tend to be oxidized photolytically or by pH-changes. In the pharmaceutical industry, CDs are used as drug-delivery systems. CDs can be protective agents, and aid in solubility and transport properties for poorly soluble drugs. CDs are commonly used in chromatographical methods, where they act as complexants for molecules to be analyzed. CDs can be used both added to the mobile phase, and covalently bonded to the stationary phase, with particular emphasis on separation of enantiomers (Steed and Atwood (2000)).

Because of the interesting properties, applications may be expanded by chemically modifying CDs. For example, modification with mercaptoundecane sulfonic acid has led to broad-spectrum, non-toxic, virucidal action in mice and in cultured human cells (Jones et al. (2020)). Also, the hydrophilicity of CDs have been exploited by attaching them to a reverse osmosis membrane, which nearly tripled the water permeance while keeping the high ion-rejection compared to unmodified membrane. This being potentially useful for desalination of water in areas with limited fresh-water (Wu et al. (2022)). In light of these applications, a hypothesis of this master's thesis is that CD-terephthalate ester can be synthesized in a similar way as proposed for cellulose (Figure 4), and potentially complement some of them, or find its own niche. CDs' uptake of different compounds is also a topic of interest, especially regarding uptake of pollutants, where CDs were successfully used to rapidly complex with some representative aromatic carcinogens, a pesticide, plastic additives, and pharmaceuticals (Alsbaiee et al. (2016)). The negatively charged carboxylate of a conjugated CD-terephthalate can perhaps be used to modify complexation with charged molecules through attraction or repulsion, and even respond to changes in pH.

1.3.4 Cyclodextrins as Rate-Enhancers in Enzymatic Degradation of PET

High degradation rate is one of the biggest objectives for engineering an enzymatic degradation process for PET. Enzymatic degradation of PET to its monomers are described in Figure 6. One of the bottlenecks for this is product inhibition. The PET degradation products mono-(2-hydroxyethyl) terephthalate (MHET) and bis-(2-hydroxyethyl) terephthalate (BHET) have been shown to competitively inhibit the *Thermobifida fusca* cutinase TfCut2 (Barth, Oeser et al. (2015)). It is assumed that the FsC is also affected by product inhibition.

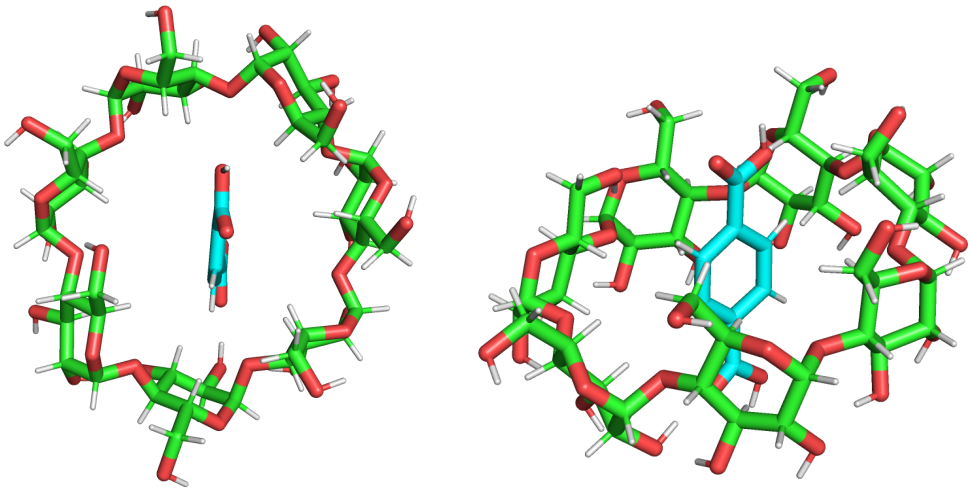

Figure 7: Illustration of the inclusion complex β-CD:TPA, made with PyMOL based on atomic coordinates.

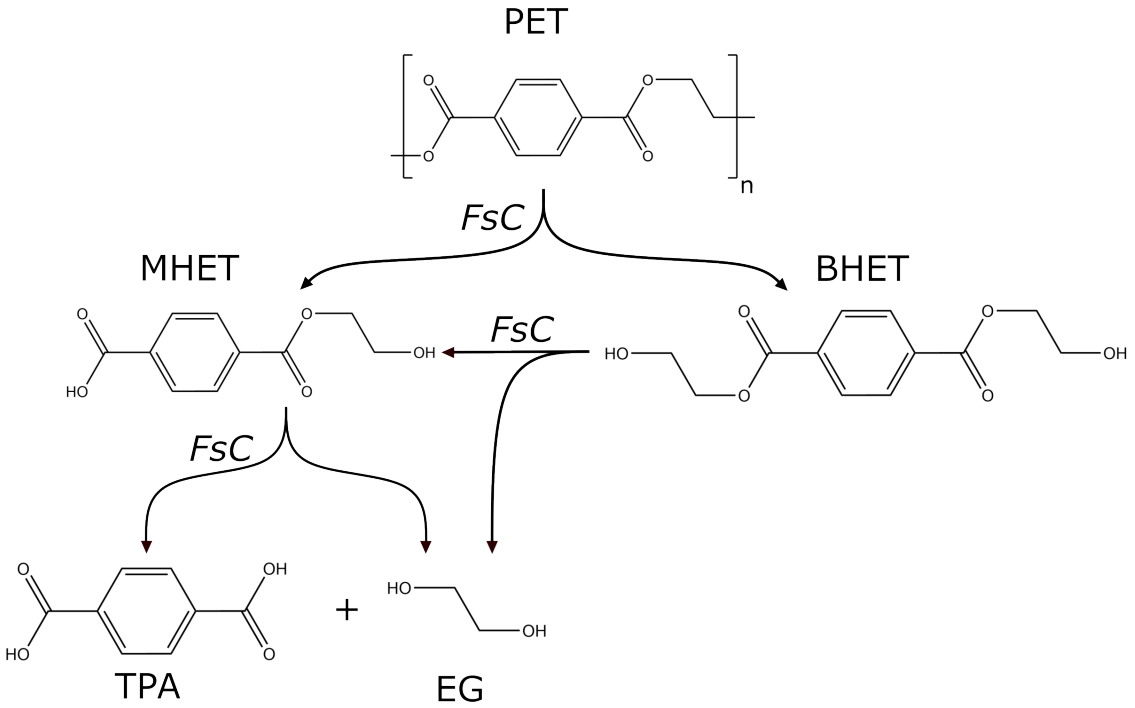

Figure 6: Scheme of enzymatically catalyzed reactions by FsC (*Fusarium solani* cutinase) in the degradation of PET (poly (ethylene terephthalate)) to monomers MHET (mono-(2-hydroxyethyl) terephthalate), BHET (bis-(2-hydroxyethyl) terephthalate), TPA (terephthalic acid), and EG (ethylene glycol).

In this master's thesis, cyclodextrins were investigated as means to keep BHET, MHET, and TPA from interfering with the PET-degrading enzyme, FSC, as highlighted in Figure 2. The hypotehsis is that CDs form inclusion complexes with the aromatic degradation products from PET, as illustrated with TPA in Figure 7, and this will keep the degradation products from occupying the enzyme.

1.4 Background for analytical tools

In this section, theoretical background for the two spectroscopic techniques Nuclear Magnetic Resonance (NMR) and Fourier Transform Infrared (FTIR) spectroscopy is provided. In this thesis, NMR and FTIR were used to characterize chemical reaction products, measure inclusion complex formation, and monitor product concentration developments in enzymatic degradation of PET.

1.4.1 NMR Background

NMR spectroscopy has become one of the most important spectroscopic techniques for the determination of molecular structures. An NMR-spectrum can reveal much information about different atoms' chemical environments, which is one of the reasons for the popularity of the method.

This introduction to NMR is simplified, but detailed enough to understand the experiments and results in the scope of this master's thesis. Because this section summarizes well-documented principles based on Friebolin (2011) and Silverstein et al. (2014), no direct references are used.

The foundation for NMR comes from the inherent nuclear property called angular momentum, which relies on nuclei being assumed to be spherical. The angular momentum of a nucleus is in fact quantized, and is described by the angular momentum quantum number, often called the nuclear spin, symbolized by the letter I. The spin of a nucleus can take values $I = 0, 1/2, 1, 3/2, 2, ...$, with 6 being the highest. The spin cannot yet be predicted from theory.

The angular momentum is associated with a property called magnetic moment, and these two are proportional to each other, by a proportionality factor called the magnetogyric ratio. A high magnetogyric ratio means that the nucleus is sensitive to detection, while a low number means it is insensitive.

Spin $I = 0$ gives no magnetic moment, and these types of nuclides are undetectable by NMR. Coincidentally, the ^{12}C and ^{16}O nuclides belong in this category. This means that the atoms comprising a large part of biomass and organic molecules cannot be observed with NMR. The ^{1}H and ^{13}C have spin $I = 1/2$, and considering nearly all hydrogens are ^{1}H and around 1% of all naturally occurring carbon nuclei are ^{13}C, organic molecules can be detected. There are also ways to enrich molecules with a higher degree of ^{13}C to enhance the sensitivity of the sample.

When a sample is to be analyzed by NMR, it is subjected to a strong external magnetic field. This aligns the otherwise randomly oriented spins of nuclei either parallel to or against the external field, but the nuclei precess around the field. Alignment parallel to the field has lower energy, leading to a higher population of nuclei, while alignment against the external field has higher energy. The differences in energies will increase with increasing external field strength, however, the population difference between the two states is very small.

Perturbing the sample with oscillating electromagnetic pulses makes nuclear spins resonate, and the frequency at which they absorb and re-emit energy is called the resonance frequency. An NMR signal is obtained by recording the electrical signal induced in a detector coil by the precessing spins. A Fourier transformation of this time-domain signal results in the resonance frequencies in a spectrum. Nuclei in different chemical environments have different resonance frequencies, also called chemical shifts, which makes NMR useful for distinguishing them. Neighboring magnetic dipoles can interact with each other, causing spin-spin coupling, which is observed as splitting of signals. The intensities of signals are proportional to concentrations, allowing determination of relative amounts of compounds.

Although NMR is the most powerful tool for polysaccharide analysis, ^{1}H-, ^{13}C-, and 2D-spectra traditionally require the sample to be soluble, which is challenging when studying large polymers like cellulose. Solid-state NMR or special solvents are required to obtain cellulose-spectra. Special solvents include DMSO-d_6/TBAF (Deuterated dimethyl sulfoxide/Tetrabutyl-ammoniumfluoridetrihydrate), ionic liquids, or salt melts (Heinze et al. (2006)).

One challenge with NMR is that water, which is commonly used as solvent or medium, can give

an intense and obstructive signal. The δ^1H signal of water at 4.7 ppm (25 ℃) can often hinder interpretation of spectra through interference with other signals. Deuteration of solvents and solvent-suppression can reduce the impact of this, but water may still be present as an impurity.

Particular NMR experiments used in this thesis, Heteronuclear Single-Quantum Coherence (HSQC), Heteronuclear Multiple Bond Correlation (HMBC), and Diffusion Ordered Spectroscopy (DOSY), give information about 1 bond ^{1}H-^{13}C coupling, 2-4 bond ^{1}H-^{13}C coupling, and diffusion of molecules, respectively.

1.4.2 FTIR Spectroscopy Background

FTIR spectroscopy is commonly used to characterize insoluble substrates such as cellulose (Lease et al. (2021)). FTIR gives information of the types of chemical bonds present in the analyte. In general, organic chemists utilize the parts of infrared light from 4000 to 400 cm^{-1} (Silverstein et al. (2014)).

Parts of the infrared spectrum of electromagnetic radiation can be absorbed by an organic molecule, and converted to molecular vibration. The absorption is quantized, and for each wavenumber in the interval, measuring the dipole change of whole molecules induced by IR radiation, a spectrum can be obtained (Silverstein et al. (2014)).

The instrument emits light containing all wavenumbers from 4000 to 400 cm^{-1}. The radiation from the spectrometer is split into two beams, one of fixed length passing through the sample, and the other with variable length for reference, using movable mirrors. The difference in lengths cause constructive and destructive interference in a pattern, which when converted with a Fourier transformation change from time to frequency domain. The resulting spectrum is absorbance or transmittance as a function of frequency (Silverstein et al. (2014)).

FTIR is primarily used to identify functional groups in a sample. Empirical comparisons and extrapolation from simpler compounds are often necessary, however, in combination with other techniques, FTIR can be a powerful tool for characterizing chemical structures (Silverstein et al. (2014)).

2 Aims of the thesis

The overall aim for the thesis was to investigate the potential uses for carbohydrates to improve a hypothetical process for the enzymatic degradation of PET plastic (Figure 2).

This aim is based on 3 hypotheses:

- Hypothesis 1: Esterification of cellulose with TPA is a feasible way to produce a new polymer with novel properties: "cellulose terephthalate".
- Hypothesis 2: TPA forms inclusion complexes with α-CD and β-CD.
- Hypothesis 3: Cyclodextrins can form inclusion complexes with PET degradation products to improve the rate of enzymatic degradation of PET by reducing product inhibition.

As a sub-objective of the thesis to test Hypothesis 1, the synthesis of a cellulose terephthalate ester was attempted by using TsCl as an activator. Several model carbohydrates were used including glucose, cellopentaose, β-cyclodextrin, and Avicel (polymeric cellulose). Cellulose terephthalate has potentially interesting properties, described in section 1.3.2.

A second sub-objective of the thesis to test Hypothesis 2 was to determine the association and dissociation constants for the α-CD:TPA and β-CD:TPA inclusion complexes. This was done by NMR titration to measure chemical shift perturbations.

A third sub-objective of the thesis to test Hypothesis 3 was to investigate whether cyclodextrins could increase the degradation rate of an FsC. This was done by degrading PET with FsC and following the developments of degradation product concentrations in an NMR tube, using time-resolved ^{1}H-NMR.

The sub-objectives describe how the thesis might contribute to finding a novel use for TPA, and also increase the PET degradation rate by reducing product inhibition, overall improving the hypothetical process described in Figure 2.

3 Materials and methods

3.1 Materials

3.1.1 Chemicals

The following chemicals were used in different parts of the thesis: glucose, pyridine, terephthalic acid (TPA) (98%, Sigma Aldrich) , cellopentaose (95%, Megazyme), cellulose (Avicel), 1-butyl, 3-methylimidazolium chloride (BMIMCl) (≥98%, Sigma Aldrich), *p*-Toluenesulfonyl chloride (TsCl) (≥99%, Sigma Aldrich), NaOH, DMSO-d_6, D_2O (99.9 atom % D), β-cyclodextrin (≥98.0%, Sigma Aldrich), α-cyclodextrin (≥98.0%, Sigma Aldrich).

All chemicals were used as recieved, with no further purification.

The Poly (ethylene terephthalate) (PET) film (0.25 mm thickness, product code ES301445, low crystallinity) for the enzymatic degradation of PET by FsC (See section 3.4.2) was obtained from Goodfellow.

3.1.2 Instruments

NMR spectra were obtained on either; a Bruker Ascend 800 MHz with Avance III HD console equipped with a 5-mm cryogenic CP-TCI z-gradient probe and SampleJet, or a Bruker 600 MHz Avance III HD equipped with a 5-mm cryogenic CP-TCI z-gradient probe and SampleCase, both at the NV-NMR laboratory at NTNU. FT-IR spectra were obtained on a Bruker ALPHA FTIR spectrometer at NTNU. Freeze-drying was performed on a Christ Beta 1-8 LDplus.

3.2 Modification of glucose, cellopentaose, cellulose and β-Cyclodextrin

Modification of carbohydrates was a key point in this project, and CTP being a main objective. Because cellulose is difficult to dissolve in traditional solvents, the smaller, soluble carbohydrates glucose and cellopentaose were used as model systems for cellulose, allowing NMR to be used for identification of products.

3.2.1 Tosylation of glucose in pyridine

10 mg glucose was reacted with 30 mg *p*-toluenesulfonyl chloride (TsCl) in 0.5 mL pyridine. The reaction was run at 70 °C for 45 minutes. Precipitation was induced by washing the mixture in acetone three times. The precipitate (0.1 mL) was later dissolved in 0.15 mL D_2O for examination using NMR. ^{1}H-NMR, HSQC and HMBC spectra were obtained on an 800 MHz spectrometer.

3.2.2 Terephthalation of glucose in pyridine

Glucose (10 mg) was dissolved in 0.5 mL pyridine, and 30 mg terephthalic acid (TPA) and 43 mg TsCl was attempted dissolved in another 0.5 mL of pyridine. Just after, the two fractions were mixed and reacted at 70 °C for 1 hour. The mixture precipitated (1 mL) and was washed in acetone 3 times, before dissolution of 0.05 mL of the precipitate in D_2O and NMR analysis. ^{1}H- and HSQC spectra were obtained on an 800 MHz spectrometer.

3.2.3 Terephthalation of glucose in BMIMCl

2.5 g of the ionic liquid 1-butyl-3-methyl-imidazolium chloride (BMIMCl) was heated in waterbath to just under 100 °C. 30 mg glucose was then dissolved, followed by 83 mg TPA. When the mixture was clear, 100 mg of TsCl was added and the mixture was stirred for two hours at the same temperature.

After the reaction, 10 mL acetone was added to the mixture in an attempt to extract some of the present compounds. The immiscible BMIMCl and acetone phases were separated using a pipette. The BMIMCl phase was mixed with ethanol to around 15 mL total, which mixed instantaneously to a homogeneous mixture. The solvents in both phases were evaporated using a rotavapor. The remaining materials were washed in water, where a precipitate formed. The precipitate was washed two more times. Water fractions were analyzed by NMR with 10% D_2O. The washed precipitates (around 0.1 mL) were air-dried overnight, and dissolved in DMSO-d_6-d_6 for NMR analysis. Analyses were done on an 800 MHz spectrometer.

3.2.4 Subsequent tosylation and terephthalation of cellopentaose in BMIMCl

Cellopentaose (18 mg) was dissolved in 2 g BMIMCl. TsCl (77 mg) was added to the solution and reacted for 2 hours at 70 to 90 °C. The resulting mixture was soluble in ethanol, methanol, isopropanol and water. TPA (42 mg) was added the next day and reacted for 1 hour 30 minutes at the same temperature.

10 mL water was added to the new sample. Precipitate formed upon water addition was centrifuged (5250 xg, 10 minutes, Allegra X-15R Centrifuge), the supernatant was saved, and the pellet was washed in 10 mL water 3 times. A part of each fraction was analyzed by NMR on an 800 MHz spectrometer, the original water fraction in water and 10% D_2O, and a pellet covering only the bottom of a 1.5 mL Eppendorf tube of solids was dissolved in 0.15 mL DMSO-d_6. The rest of the water fraction was freeze-dried, resulting in 0.1 mL of solids. The freeze-dried solids were dissolved in 0.6 mL DMSO-d_6 and analysed by NMR on a 600 MHz spectrometer.

3.2.5 Tosylation and terephthalation of cellulose in BMIMCl with pyridine as co-solvent

Cellulose (0.2 g) was dissolved in magnetically stirred BMIMCl (3.0 g) for 18 hours at 80-90 °C. The mixture was then added 1 mL of pyridine while 0.7 g TsCl was dissolved in another 1 mL of pyridine for 15 minutes. TsCl in pyridine was added dropwise within 5 minutes. The reaction was run at 40-50 °C for 8 hours. The product was precipitated in 50 mL ethanol, then filtered and washed with 20 mL ethanol, 20 mL water, and again three times with ethanol. It was left to dry in a fume hood overnight. FTIR spectrum was recorded for a 2x2x1 mm sample of the tosylated cellulose (TOSC) using a Bruker ALPHA FTIR spectrometer.

A 1x1x0.5 cm piece of TOSC was dissolved in BMIMCl and mixed with 0.2 g TPA dissolved in BMIMCl, and reacted for 4 hours at 70-90 °C. The mixture was then carefully precipitated in ethanol, and washed with water and ethanol again. It was filtrated and dried overnight, and formed a flaky material. FTIR spectroscopy was done on a 2x2 mm flake of the product using a Bruker ALPHA FTIR spectrometer.

3.2.6 Tosylation of β-Cyclodextrin

0.2 g β-CD was dissolved in 25 mL dry pyridine, and 0.5 g TsCl was added. The reaction was run for 40 minutes at room temperature, according to (Melton and Slessor (1971)). To stop the reaction, around 75 mL of water was added. Water and pyridine were evaporated three times until there was no smell of pyridine. A 50 μL sample of the remaining syrup was dissolved in D_2O and analysed by NMR on an 800 MHz spectrometer.

3.2.7 NaOH-activated terephthalation of tosylated β-Cyclodextrin

20 mg of TPA was dissolved in 0.2 mL 1 M NaOH and added to 5 mL water. Around 0.3 mL of pre-made CD-Ts was added dropwise. The mixture was reacted at 30-50 °C for 20 hours. The suspension was centrifuged (5250xg, 25 min, Allegra X-15R Centrifuge) and washed with water, and centrifuged (5250xg, 15 min, Allegra X-15R Centrifuge) and washed 2 more times. The samples were freeze-dried. 0.1 mL of the precipitate was dissolved in 0.5 mL d6-DMSO-d_6 for NMR, while all solids from the supernatant was dissolved in D_2O. ^{1}H and ^{1}H-^{13}C HSQC and HMBC spectra were obtained for both products. Diffusion ordered spectroscopy (DOSY) was also performed to get additional information about conjugation, exploiting the slower diffusion of CD compared to smaller molecules. All NMR analyses for this experiment was done on a 600 MHz spectrometer.

3.3 Inclusion complex with cyclodextrin and terephthalic acid

3.3.1 Association constant of β-CD:TPA inclusion complex

Different molar ratios of CD:TPA were investigated by NMR-spectroscopy on a 600 MHz spectrometer to determine the association constant. Table 1 shows the concentrations and ratios used to measure the association constant for the β-CD:TPA inclusion complex. The changes in ^{1}H chemical shifts of CD were measured using ^{1}H-^{13}C HSQC spectra, plotted against concentration of TPA, and a two-state exchange model (Equation 3) was fitted to the data. A Python-script used to fit the two state model to $\Delta\delta^1$H for each proton, and calculate K_a and K_d can be found in https://github.com/gcourtade/masters/tree/main/2023/AHB_CD_PET.

Table 1: Concentrations of β-Cyclodextrin and terephthalic acid in 50 mM pH 8 sodium phosphate buffer for determination of association constant.

Sample	**Concentration CD [mM]**	**Molar ratio TPA**	**Concentration TPA [mM]**
Control	1.5	0	0
1	1.5	0.4	0.6
2	1.5	0.9	1.3
3	1.5	1.2	1.7
4	1.5	1.8	2.6
5	1.5	2.6	3.8
6	1.5	3.9	5.8
7	1.5	14.3	21

3.3.2 Association constant of α-CD:TPA inclusion complex

As for β-CD, different molar ratios of CD:TPA were investigated by NMR-spectroscopy on a 600 MHz spectrometer to determine the association constant. Table 2 shows the concentrations and ratios used to measure the association constant for the α-CD:TPA inclusion complex. A Python-script used to fit the two state model (Equation 3) to $\Delta\delta^1$H for each proton, and calculate K_a and K_d can be found in .

Table 2: Concentrations of α-Cyclodextrin and terephthalic acid in 50 mM pH 8 sodium phosphate buffer for determination of association constant.

Sample	Concentration CD [mM]	Molar ratio TPA	Concentration TPA [mM]
Control	1.5	0	0
1	1.5	0.4	0.6
2	1.5	0.9	1.3
3	1.5	1.2	1.7
4	1.5	1.8	2.6
5	1.5	2.5	3.7
6	1.5	3.9	5.7
7	1.5	5.4	7.9

3.4 Product inhibition of FsC

3.4.1 Production of FsC

Protein production was carried out according to procedure described by Hellesnes et al. (Hellesnes et al. (2023)). Cell culture of recombinant *E. coli* ER2566 with plasmid pFCEX1D containing wild-type FsC were incubated in 5 mL precultures. The precultures contained LB supplemented with 100 μg/mL ampicillin. Incubation took place at 30 ℃and 225 rpm for 16 h. Main cultures were made by inoculating 500 mL of 2×LB (20 g/L tryptone, 10 g/L yeast extract, 5 g/L NaCl) with 1% preculture, followed by incubation at 25 ℃and 225 rpm. Induction of cells with 0.1 mM isopropyl-β-d-thiogalactopyranoside was done at $OD_600 = 1.7–1.9$. After being induced, cells were incubated at 225 rpm and 25 ℃overnight.

The cells were harvested by centrifugation for 5 minutes at 5000xg at 4 ℃. The pellet was carefully resuspended in 35 mL of spheroplast buffer (100 mM Tris HCl pH 7.5, 500 mM sucrose, 0.5 mM EDTA) with a protease inhibitor tablet (cOmplete^{TM} ULTRA protease inhibitor tablet). The suspension was centrifuged for 10 minutes and 5 minutes more at 6500xg. The supernatant was kept on ice, from now called "Spheroplast fraction". 35 mL MilliQ water was added to the pellet, which was carefully resuspended. The new suspension was centrifuged for 45 minutes at 45000xg. The new supernatant was kept on ice, from now called "Water fraction".

The spheroblast and water fractions were sterile filtered with a 0.2 μm syringe filter. 2 mL 0.5 M NaAc pH 5-buffer was added to the water fraction and mixed. The solution was centrifuged for 20 minutes at 45000xg, and sterile filtered. Sample was purified with FPLC (HiTrap CM FF 5 mL column, 5 mL/min flow rate, buffer 50 mM NaAc pH 5, linear gradient 0-50% with same buffer but 1 M NaCl in addition)

3.4.2 Investigation of the effect of cyclodextrins on PET degradation rate of a wild-type FsC using time-resolved NMR

The effect of cyclodextrins on PET degradation rate of FsC was studied using time-resolved ^{1}H-NMR, recording a solvent-suppressed ^{1}H-spectrum every 5 minutes for 16 hours at 313 K on a Bruker 800 MHz NMR-spectrometer, a total of 204 proton-spectra.

Three samples contained 10 μM of FsC, 25 mM sodium phosphate, 50 mM NaCl, at pD 6.5 in 96% D_2O. In addition, one contained 1.65 mM β-CD, one contained 1.55 mM α-CD, and the control contained no cyclodextrin. Each 600 μL sample also contained 5 μL D_2O with 0.75% TSP (trimethylsilyl propanoic acid) to be used as internal standard for integration of relevant peaks. Final concentration of FsC was 10 μM for all three samples.

Integrals for relevant regions (BHET, MHET, and TPA peaks) were done for all individual ^{1}H-spectra using the TopSpin command *intser* (Serial integration) with respect to the calibrated internal standard and plotted against time. Python-script used to plot the integrals over time can be found in https://github.com/gcourtade/masters/tree/main/2023/AHB_CD_PET.

4 Results

4.1 Chemical modification of glucose, cellopentaose, cellulose and β-Cyclodextrin

This section describes results of attempts to conjugate carbohydrates to TPA, imagining CTP as a potentially useful material. Glucose and cellopentaose were used as soluble analogs of cellulose to enable NMR analyses. Because of the many experiments and different results, all key experimental results reported in section 4.1 are summarized in Table 3.

The different procedures described in section 3.2 describe systems of various solvents and molecules with different degrees of solubility. It is important that observations like precipitation or viscosity changes are reported in this section to interpret the results. Because of this, qualitative observations that may have affected the reactions are mentioned throughout section 4.1.

Table 3: Overview of results presented in section 4.1, from the chemical modification of glucans. Reaction numbers, reactants present, physical observations, and information obtained spectrophotometrically are listed.

Reaction number	Reactants	Observations	Information from NMR/FTIR
1	Glucose, pyridine, TsCl	Color change	Different H6 peaks indicate tosylation occurred
2	Glucose, pyridine, TsCl, TPA	Color and viscosity change	Different H6 peaks indicate a reaction
3	Glucose, BMIMCl, TsCl, TPA	Color change Water precipitation in both acetone and BMIMCl phase	No indication of reaction
4	Cellopentaose, BMIMCl, TsCl, TPA	Color change	No indication of reaction
5	Cellulose, BMIMCl, TsCl, TPA, pyridine	Color change Clear gel-like, maleable precipitate Flaky precipitate	FTIR spectrum indicates tosylation may have occurred
6	beta-CD, pyridine, TsCl	Color change	Different H6 peaks indicate tosylation occurred
7	beta-CD, water, NaOH, pyridine, TsCl, TPA	White precipitation	Different H6 peaks and similar diffusion coefficients indicate tosylation occurred

4.1.1 Tosylation of glucose in pyridine

For the tosylation of glucose in pyridine, Reaction 1 (Table 3) (See Section 3.2.1), HSQC and HMBC NMR-analyses was performed on the product from Reaction 1 (Table 3). The top panel of Figure 8 shows NMR signals for pyridine (a (8.5 ppm, 147 ppm), b (8 ppm, 128 ppm), c (8.7 ppm, 142 ppm)), tosyl group (d (7.7 ppm, 126 ppm), e (7.3 ppm, 130 ppm), and f (2.3 ppm, 21 ppm)), along with unassigned glucose signals.

Signals a to f from the top panel of Figure 8 were expanded upon in Figures A.1 and A.2. HMBC correlations between pyridine and glucose shown in Figure A.1 indicated reaction at C6 and C1 of glucose. Three compounds, labelled i, ii, and iii in Figure A.2 were assigned as pyridine, pyridine

reacted at C6 of glucose, and pyridine reacted at C1 of glucose, respectively. Three compounds, labelled iv, v, and vi in Figure A.2 were three distinguished types of tosyl groups, but they were not fully assigned.

As shown in the bottom panel of Figure 8, four different glucose CH_2-signals were present, labelled a (3.7 ppm, 61 ppm), b (4.35 ppm, 69.5 ppm), c (4.8 ppm, 62 ppm), and d (3.85 ppm, 44 ppm). Signal a was assigned by comparison of assigned chemical shifts for glucose (Silverstein et al. (2014)), signal b was assigned by comparison with chemical shifts for tosylated glucans (Heinze et al. (2006)), signal c was assigned by HMBC correlation shown in Figure A.1, while signal d was assigned by comparison of chemical shifts with chlorinated cellulose (Gao et al. (2018)).

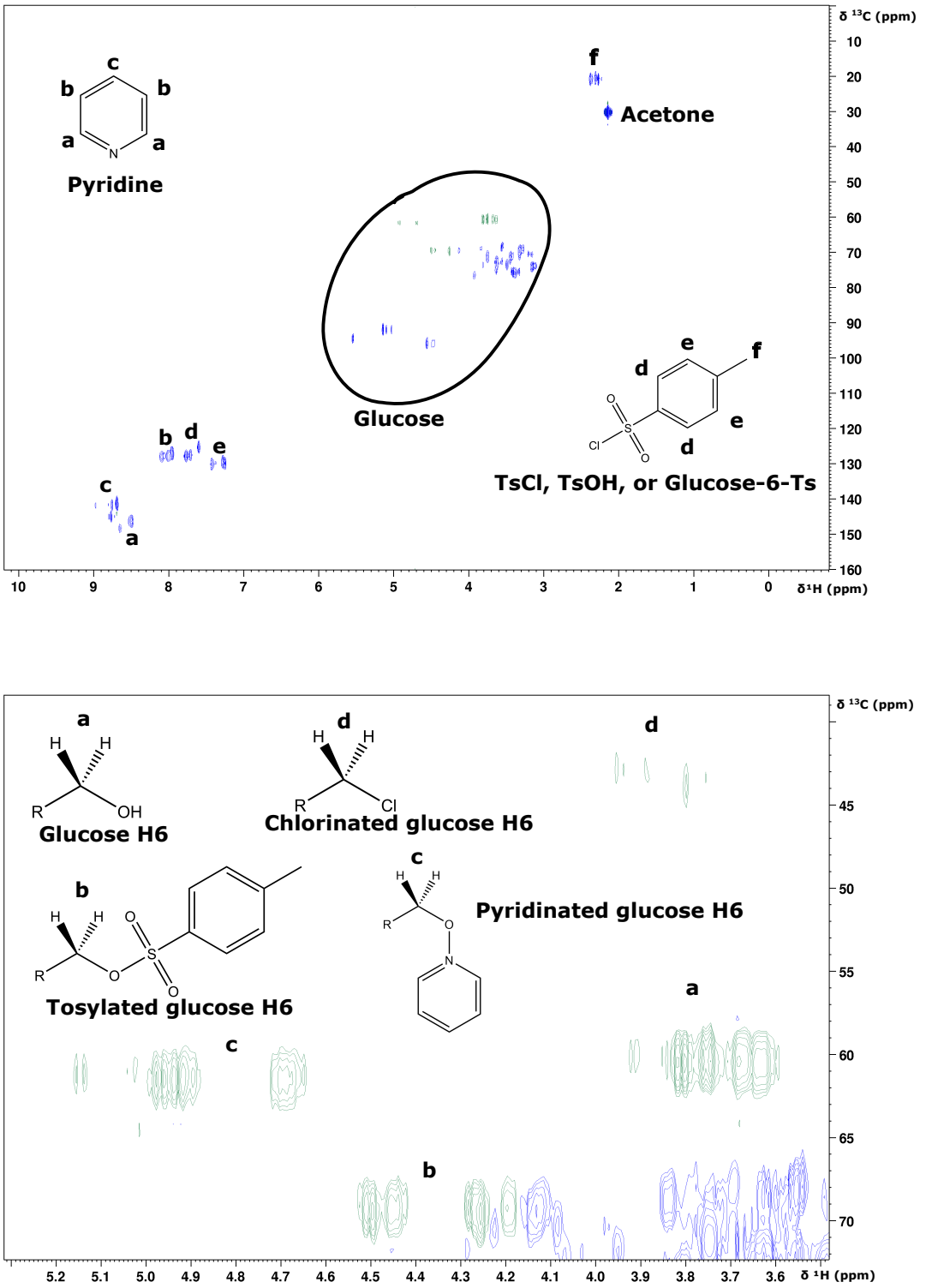

Figure 8: HSQC-spectrum of the product of Reaction 1 (Table 3), dissolved in D_2O. Blue signals are CH- and CH_3-hydrogens, while green signals are CH_2-hydrogens. Top: Overview of complete spectrum. Signals were assigned for pyridine (a (8.5 ppm, 147 ppm), b (8 ppm, 128 ppm), c (8.7 ppm, 142 ppm)) and tosyl groups (d (7.7 ppm, 126 ppm), e (7.3 ppm, 130 ppm), f (2.3 ppm, 21 ppm)). Bottom: Area of interest showing different glucose CH_2-signals labelled a (3.7 ppm, 61 ppm), b (4.35 ppm, 69.5 ppm), c (4.8 ppm, 62 ppm), and d (3.85 ppm, 44 ppm). Recorded at 298 K.

4.1.2 Terephthalation of glucose in pyridine

For Reaction 2 (Table 3) (See section 3.2.2 for methods), there were problems with precipitation. TPA was more difficult to dissolve in pyridine than glucose, which may have led to low concentrations of TPA in the solution, making conjugation unlikely. As the pyridine was mixed with TPA and TsCl, there was formed a white, viscous mixture.

HSQC spectra in Figure B.1 (Bottom) showed strong signals from pyridine (a (8.6 ppm, 142 ppm), b (7.8 ppm, 127 ppm), c (8.3 ppm, 146 ppm)) and tosyl-protons (e (7.5 ppm, 126 ppm), f (7.1 ppm, 130 ppm), as well as a weak signal for TPA (d (7.7 ppm, 129 ppm)). The top panel of Figure B.1 shows glucose CH_2 signals a (3.7 ppm, 61 ppm) and b (4.46 ppm, 64 ppm). The chemical shifts of signal a corresponds to H6 of glucose, while signal b with different chemical shifts may originate from a conjugated glucose molecule, indicating a reaction.

4.1.3 Terephthalation of glucose in BMIMCl

To gain insight on how a reaction would occur in BMIMCl, glucose was reacted with TsCl and TPA in Reaction 3 (Table 3). Separation led to different fractions, treated as described in section 3.2.3.

During the first hour of the reaction, the colour of the mixture changed gradually from light yellow to brown. When acetone was added to try and extract some compounds, the phases seemed immiscible, and the acetone fraction changed colour from clear to a low intensity of brown colour seen in the original mixture.

The different fractions from Reaction 3 were analysed by NMR, and revealed where the different compounds had remained. All spectra from Reaction 3 were obstructed by impurities, and are therefore not shown.

From the acetone extract, the water fraction contained BMIMCl and TsCl, and some very weak glucose signals, mostly masked by BMIMCl-signals. The water precipitate from the acetone fraction contained TPA and TsCl, as well as BMIM-Cl with some possible contamination.

From the BMIMCl-phase, the water fraction showed intense BMIMCl-signals, as well as some less intense signals from TsCl, and ethanol from the cleanup process. There were also some glucose signals in the HSQC spectrum of the water fraction of the BMIMCl-phase, annotated as a (5.15 ppm, 90 ppm), b (4.6 ppm, 95 ppm), and c (3.7 ppm, 60 ppm) in Figure C.1. Signals a and b were from anomeric protons, while signal c was from H6 of glucose. Here, H6 had its unmodified chemical shift (3.7 ppm, 60 ppm). The water precipitate from the BMIMCl-phase dissolved in DMSO-d_6 displayed signals from BMIMCl, TPA, and very weak signals for TsCl and ethanol.

4.1.4 Subsequent tosylation and terephthalation of cellopentaose in BMIMCl

HSQC spectra were obtained for Reaction 4. After precipitation in water, the precipitate was freeze-dried and the supernatant was analysed with NMR. The supernatant contained BMIMCl and TsCl, but the spectrum was too crowded around the water-peak and the CH_3- and CH_2-signals of BMIMCl to identify sugar-signals. The freeze-dried precipitate was dissolved in DMSO-d_6, and showed a TPA-signal, as well as signals for BMIMCl and TsCl. Very weak sugar-signals were visible in the HSQC-spectrum belonging to the freeze-dried precipitate dissolved in DMSO-d_6, but they were too weak and obstructed to confirm reaction. Weak sugar signals are shown in the top panel of Figure D.1 in the appendix, where signal a (3.5 ppm, 60.5 ppm) was assigned as H6 of cellopentaose. In the bottom panel of Figure D.1, signals for BMIMCl (a (8.42 ppm, 136 ppm), b (7.14 ppm, 123 ppm), c (7.19 ppm, 122 ppm)) and TsCl (d (7.35 ppm, 126 ppm), e (7.04 ppm, 130 ppm)) are shown.

Due to the impurity of the products, no evidence of reaction was found in the other fractions.

4.1.5 Tosylation and terephthalation of cellulose in BMIMCl with pyridine as co-solvent

For Reaction 5 (Table 3), cellulose was reacted with TsCl in BMIMCl first, and the product was redissolved in BMIMCl for reaction with TPA, according to section 3.2.5. Cellulose dissolved in BMIMCl formed a viscous mixture, which changed colour from clear to yellow and brown after TsCl was added.

Addition of ethanol after tosylation caused rapid precipitation, and the precipitate appeared somewhat transparent and gel-like, except it seemed mouldable. TOSC was not soluble in DMSO-d_6. Instead, TOSC was analysed by FTIR spectroscopy and yielded the spectrum shown in Figure E.1 in the appendix.

FTIR (cm^{-1}): 3340 (OH stretch), 2875 (CH_2 symmetric stretch), 1635 (Adsorbed water), 1571 (Aromatic ring stretch), 1163 (C-O-C antisymmetric stretch), 1109 (Pyranose ring antisymmetric stretch), 1057 (C-O stretch), 1033 (C-O stretch), 1011 (C-O stretch), 753 (C-Cl stretch).

After the reaction between tosylated cellulose and TPA, the precipitated and filtered product was a flaky material. The resulting product would not dissolve in DMSO-d_6. This product was also analysed by FT-IR spectroscopy, and the spectrum is shown in Figure E.1 in the appendix.

FTIR (cm^{-1}): 3336 (OH stretch), 2872 (CH_2 symmetric stretch), 1671 (TPA C=O stretch), 1572 (Aromatic ring stretch), 1161 (C-O-C antisymmetric stretch), 1110 (Pyranose ring antisymmetric stretch), 1055 (C-O stretch), 1032 (C-O stretch), 1017 (C-O stretch).

4.1.6 Tosylation of β-Cyclodextrin

Reaction 6 was performed as described in section 3.2.6. Addition of TsCl turned the solution yellow instantly. During the reaction, the color faded towards light brown. The resulting product after evaporation of pyridine was a viscous syrup like liquid, with a more intense brown color.

The product from Reaction 6 was dissolved in D_2O and analysed with NMR. Signals of β-CD are shown in Figure 9, where two distinct signals for H6 are marked a (3.7 ppm, 60 ppm) and b (4.2 ppm, 70 ppm). Full spectrum is shown in Figure F.1 in the Appendix, where signals for pyridine (a (8.6 ppm, 141 ppm), b (7.9 ppm, 127 ppm), c (8.5 ppm, 147 ppm)) and tosyl group (d (7.5 ppm, 125 ppm), e (7.1 ppm, 130 ppm), f (2.2 ppm, 20 ppm)) are shown.

4.1.7 NaOH-activated terephthalation of tosylated β-Cyclodextrin

Mixing tosylated β-CD in the solution with NaOH activated TPA turned the solution white, and gave a white precipitate in the reaction mixture that sank when stirring was stopped. The precipitate and the liquid phase were separated by centrifugation as described in section 3.2.7.

The supernatant's HSQC spectrum contained signals for pyridine, TsCl and β-CD. Two versions of a toluenesulfonyl-group were distinguishable, and at least two versions of H6 of β-CD were observed. No TPA signal was present in the spectrum, which is why it was not shown.

The precipitate from the terephthalation of β-CD was dissolved in DMSO-d_6 and the aromatic region of the HSQC spectrum of this product is shown in Figure 10.

Diffusion order spectroscopy (DOSY) was also performed for the product of Reaction 7. The ^{1}H-peaks readily identified, that corresponded to previously assigned ^{1}H-^{13}C-HSQC peaks were assigned a diffusion coefficient (D). The diffusion coefficients β-CD estimated from different protons from the terephthalation of β-CD were given in Table G.1 in the appendix. H2, H3, and H5 peaks were not straight forward to distinguish from each other, and were not assigned diffusion coefficients. For all except the anomeric protons, the D given by β-CD protons were between 2 and 3 $\times 10^{-11}$ m^2/s. For a set of Ts protons at 2.39 ppm, 7.41 ppm, and 7.73 ppm, D was estimated as 2.4, 2.9, and 2.1 $\times 10^{-11}$ m^2/s respectively, and because the values are so similar to D for β-CD, it

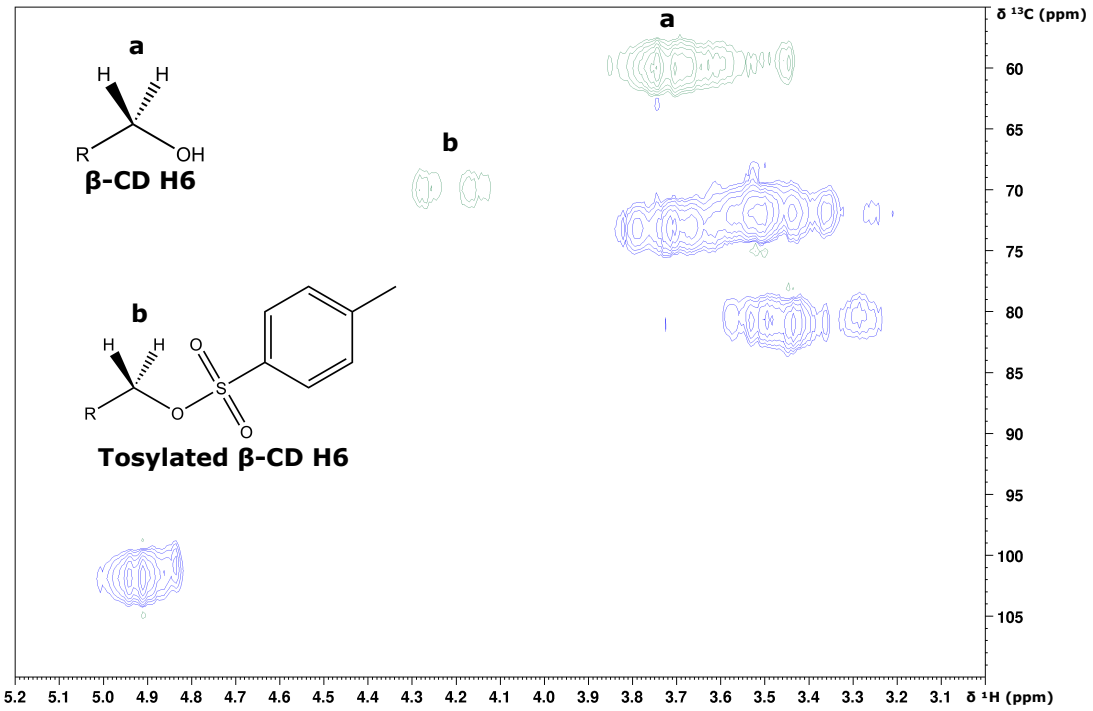

Figure 9: Region containing signals of β-CD in a HSQC spectrum of the product of Reaction 6 (Table 3) dissolved in D_2O. Signals a (3.7 ppm, 60 ppm) and b (4.2 ppm, 70 ppm) correspond to β-CD H6 protons and tosylated β-CD H6, respectively. Recorded at 298 K.

is reasonable to assume they are signals from a tosyl group attached to β-CD. A different set of Ts protons at 2.28 ppm, 7.12 ppm, and 7.50 ppm gave higher values for D, 5.7, 6.7, and 8.3 $\times 10^{-11}$ m^2/s respectively. For the proton signal from TPA at 8.04 ppm, D was estimated to 4.2 $\times 10^{-11}$ m^2/s for TPA. The results strongly indicates successful tosylation of β-CD. Having a factor of 2 different diffusion coefficient and no HMBC connection between the two molecules, esterification between TPA and β-CD had most likely not happened.

4.2 Cyclodextrin:Terephthalic acid inclusion complex

4.2.1 Determination of association constant for the inclusion complex β-CD:TPA

To assess the possibility of using β-CD to improve an enzymatic degradation of PET, the association constant for the β-CD:TPA inclusion complex was estimated by NMR titration, with concentrations given in Table 1 in section 3.3.1.

As can be seen in Figure 11, the chemical shift of all β-CD protons decreased when increasing concentration of TPA from 0 to 21 mM. While H1, H2, and H3, and H4 and H6 experienced similar changes to their chemical shift, H5 decreased the most. The changes in chemical shifts were then plotted (Raw data in Table H.1), and a two-state exchange model (Equation 3) was fitted to the observed changes and is shown in Figure 12. This allowed determination of the dissociation constant (K_d) and the association constant (K_a) for the inclusion complex, as reported by each β-CD proton.

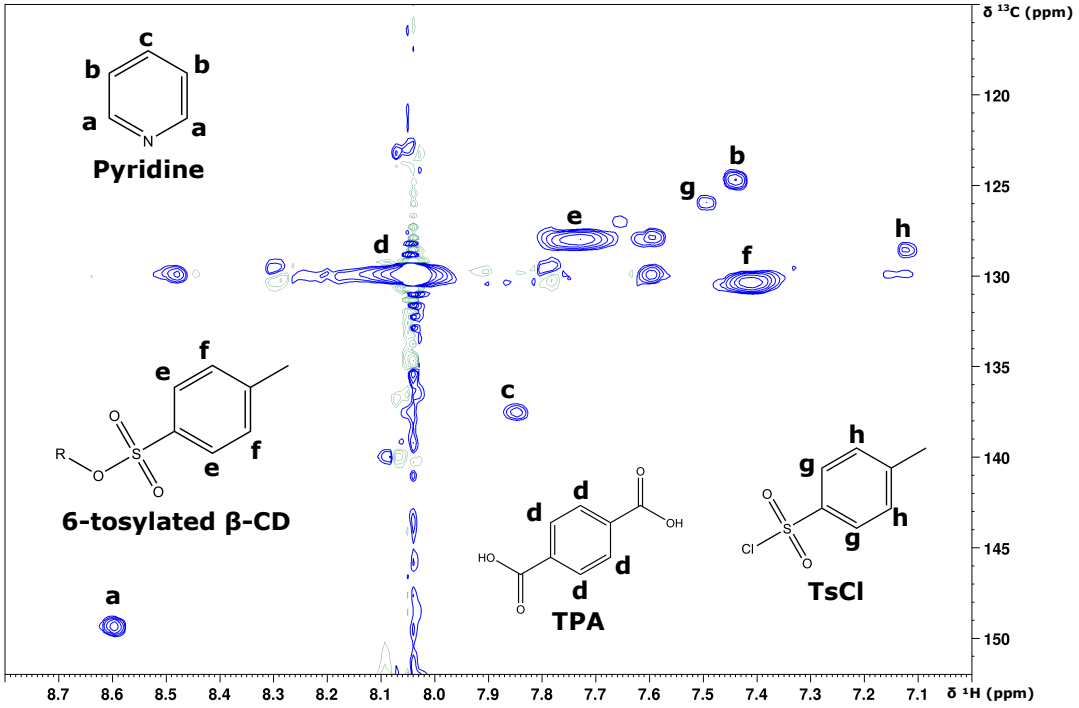

Figure 10: Aromatic region of a HSQC spectrum of the precipitate from Reaction 7, dissolved in DMSO-d_6. Signals for pyridine (a (8.6 ppm, 150 ppm), b (7.4 ppm, 125 ppm), c (7.85 ppm, 138 ppm)), TPA (d (8 ppm, 130 ppm)), tosylated β-CD (e (7.7 ppm, 128 ppm), f (7.4 ppm, 130 ppm))(R-group is β-CD), and TsCl (g (7.5 ppm, 126 ppm), h (7.1 ppm, 128 ppm)) are annotated. Recorded at 298 K.

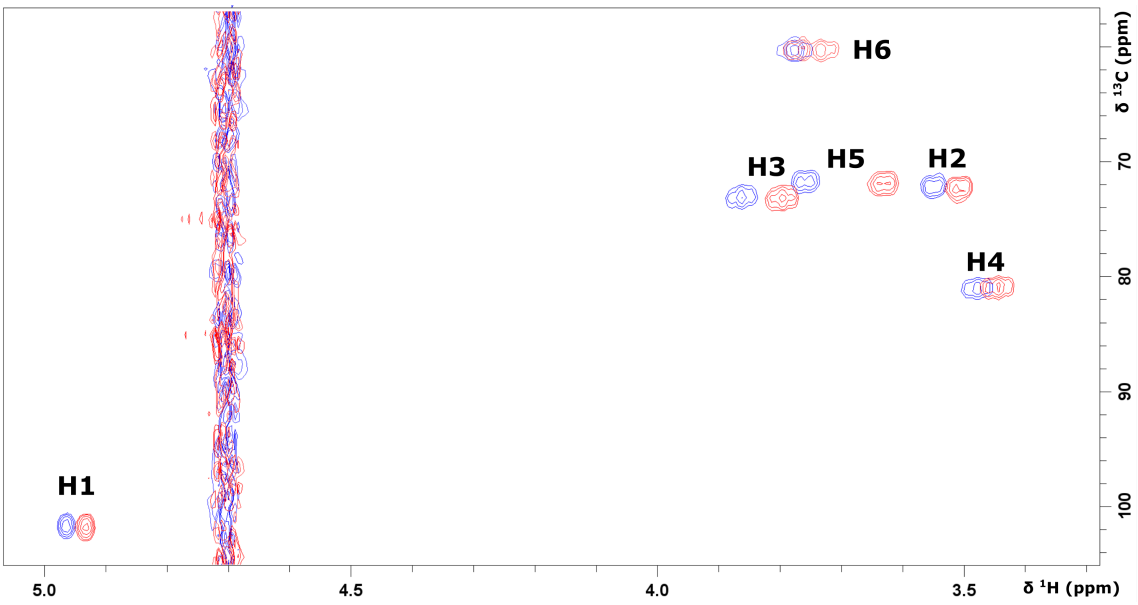

Figure 11: Overlaid HSQC spectra for the β-CD:TPA inclusion complex indicating the change in chemical shifts for different β-CD hydrogens. Blue is 1.5 mM β-CD without any added TPA, red is 1.5 mM β-CD with the highest concentration of TPA measured; 21 mM. Recorded at 298 K in 50 mM sodium phosphate buffer at pH 8.

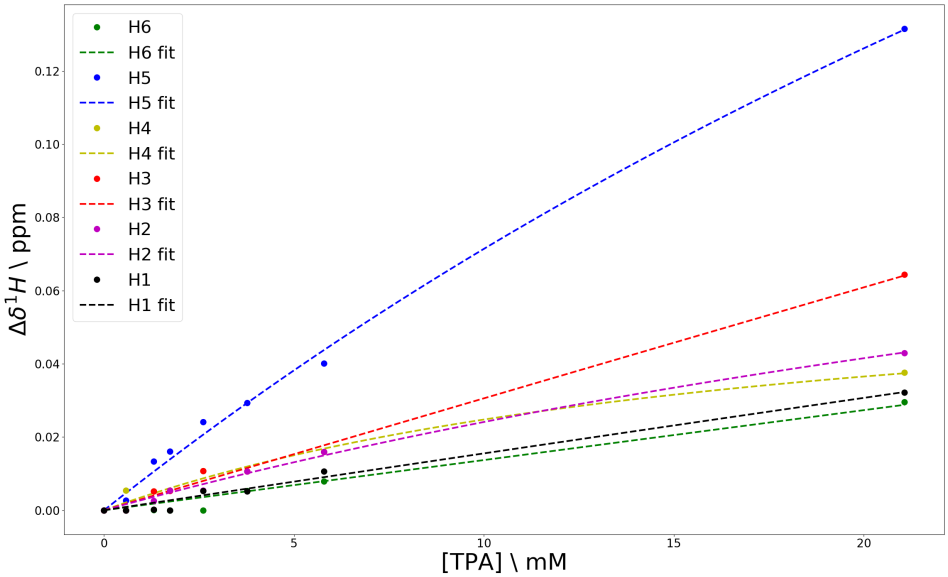

Figure 12: Change in chemical shifts ($\Delta\delta^1 H$) for β-Cyclodextrin hydrogens (points) as function of concentration of TPA. Found by NMR titration, euclidean distances were taken from each chemical shift relative to the control sample with only 1.5 mM β-CD and 0 mM TPA. A two state exchange model (Equation 3)(Dashed lines) was fitted to the data points for each hydrogen.

The appearance of the curves in Figure 12 is varied. The fit for H5 is visibly curved, while less curvature is seen for the least responsive protons, H1 and H6. The second most responsive proton, H3, also gave a less curved line than H5. Values for K_a for all β-CD protons are given in Table 4. The table also shows the maximum change in chemical shift, $\Delta\delta^1 H_{max}$, (see Equation 3).

The curves in figure 12 confirmed that H5 stood out as the most responsive β-CD proton to changes in concentration of TPA. The calculated value for K_a reported by H5 was 16 M^{-1} and K_d was 63 mM, as seen in Table 4. Doing jackknifing to estimate an error led to $K_d = 57 \pm 20$ mM.

Table 4: Estimates of dissociation and association constants, along with $\Delta\delta^1 H_{max}$, for the terephthalic acid:β-Cyclodextrin inclusion complex from changes in the chemical shift of different hydrogens in β-Cyclodextrin with varying concentration of terephthalic acid.

H no.	$\mathbf{K}_d$ **[mM]**	$\mathbf{K}_a$ **[M^{-1}]**	$\Delta\delta^1 H_{max}$ **[ppm]**
1	827	1.2	1.3
2	50	20	0.15
3	2323	0.43	7.14
4	16	61	0.07
5	63	16	0.53
6	3563	0.28	4.90

4.2.2 Determination of association constant for the inclusion complex α-CD:TPA

The association constant for the α-CD:TPA inclusion complex was estimated to gain insight of the applicability of α-CD to improve enzymatic degradation of PET by FsC. K_a was estimated by NMR titration described in section 3.3.2, with concentrations in Table 2.

The comparison of HSQC spectra for the highest and lowest concentrations of TPA in the presence of α-CD is shown in Figure 13. In the figure, all except H5 of α-CD protons can be seen to decrease in chemical shifts with increasing concentration of TPA. H5 had the largest absolute change in chemical shift, closely followed by H3, both larger than the other protons. The changes in chemical shifts were plotted and the two state exchange model (Equation 3) was fit to the data, shown in Figure 14. Estimations of dissociation constant (K_d) and the association constant (K_a) for the inclusion complex, as reported by each α-CD proton was determined from the parameters of the fitted curve.

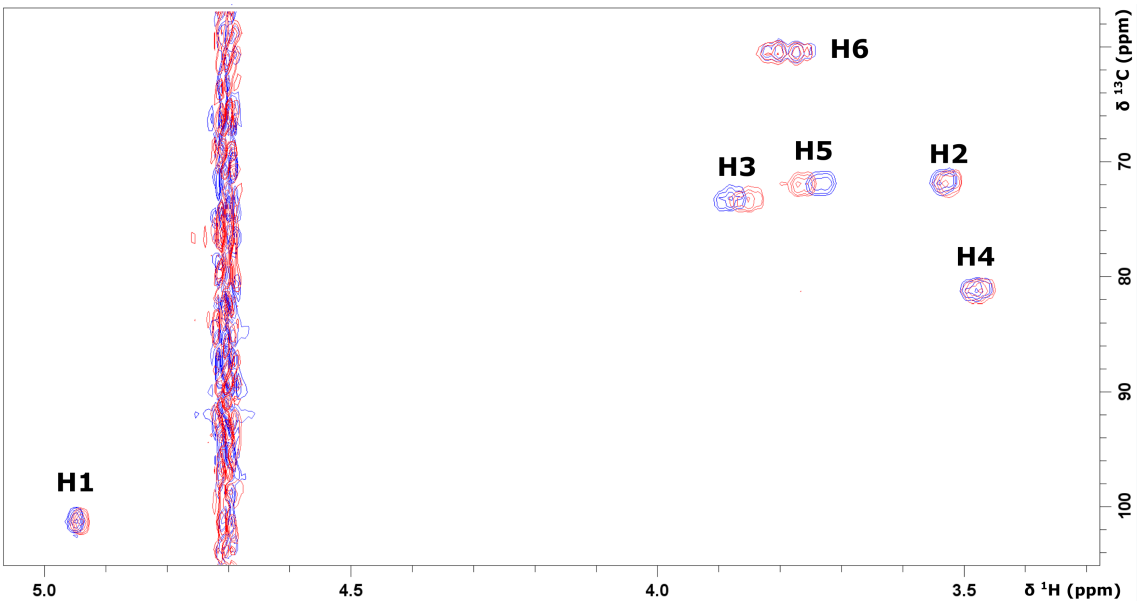

Figure 13: HSQC spectra for the α-CD:TPA inclusion complex indicating the change in chemical shifts for different α-CD hydrogens. Blue signals are from the sample with 1.5 mM α-CD, red signals are from the sample with 1.5 mM α-CD and 7.9 mM TPA. Recorded at 298 K.

As seen for β-CD, the appearances of the two state exchange model curves for α-CD protons in Figure 14 are also varied. The fit for H5 was again visibly curved, but H3 and H6 looked especially

linear. K_a and K_d values for all α-CD protons are given in Table 5. The table also shows the maximum change in chemical shift, $\Delta\delta^1 H_{max}$, (see Equation 3). H5 was also the most potent reporter of the α-CD protons in response to increasing concentration of TPA. From Table 5, K_a from H5 was given as 43 M^{-1}, while K_d was 23 mM. Jackknifing error estimation for the K_d reported by H5 led to the estimate 23 ± 7 mM.

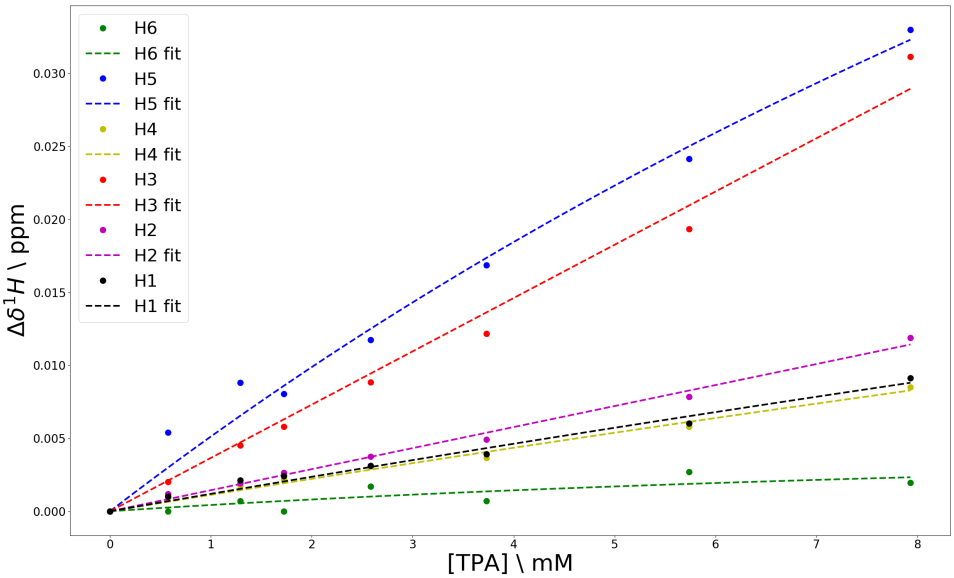

Figure 14: Change in chemical shifts ($\Delta\delta^1 H$) for α-Cyclodextrin hydrogens as function of concentration of TPA. Found by NMR titration, euclidean distances were taken from each chemical shift relative to the control sample with only 1.5 mM α-CD and 0 mM TPA. A two state exchange model (Equation 3) was fitted to the data points for each hydrogen.

Table 5: Estimates of dissociation and association constants, and $\Delta\delta^1 H_{max}$ for the TPA:α-CD inclusion complex from changes in the chemical shifts of different protons in α-CD with varying concentration of TPA.

H no.	**K_d [mM]**	**K_a [M^{-1}]**	**$\Delta\delta^1 H_{max}$ [ppm]**
1	88	11	0.11
2	3578	0.3	0.5.17
3	5327	0.2	19.48
4	88	11	0.10
5	23	43	0.13
6	12	86	0.01

4.3 Investigation of the effect of cyclodextrins on PET degradation rate of a wild-type FsC using time-resolved NMR

Recording time-resolved spectra for enzymatic degradation of PET by FsC as described in section 3.4.2 allowed investigation of the effect of CDs on the rate. The product concentrations found by serial-integration of ^{1}H-NMR peaks assigned to BHET, MHET, and TPA (Hellesnes et al. (2023))(Chemical structures and assignment shown in Figure 16) compared to an internal standard in the enzymatic degradation of PET with and without cyclodextrins present are shown in Figure 15, along with molar fractions of BHET, MHET and TPA. The values for the integrals of BHET, MHET, and TPA, along with the Python script used to make Figure 15 can be found in https:

//github.com/gcourtade/masters/tree/main/2023/AHB_CD_PET.

The sample with only FsC and PET showed a linear increase of MHET concentration, and a more exponential-looking curve for TPA concentration over the course of the experiment. The samples with FsC, PET, and CDs present showed linear increases for both MHET and TPA concentrations. For all experiments, BHET concentrations were minimal over the sampled time-period.

Development of product concentrations can give indications of an apparent degradation rate. Assuming linearity of the curves, the secant method is applied to calculate apparent degradation rate. The following apparent degradation rates were calculated by taking the difference between final and initial concentration of each product, and dividing by the time. For MHET, the apparent degradation rate in the control was calculated to 8.4 μM/h, with α-CD present it was 17.5 μM/h, and 18.9 μM/h with β-CD present. Regarding TPA, the apparent degradation rates were estimated to be 4.4 μM/h for the control, 11.2 μM/h with α-CD present, and 5.8 μM/h with β-CD present. Finally, apparent rates for BHET were 0.44, 0.33, and 0.59 μM/h for the control, with α-CD, and with β-CD, respectively.

With either of the cyclodextrins present, the final concentrations of MHET approximately doubled. Final concentrations of TPA was similar for the control and β-CD, with around double the concentration when α-CD was present. All experiments had low fractions of BHET, but β-CD gave a lower fraction of TPA than the control and α-CD.

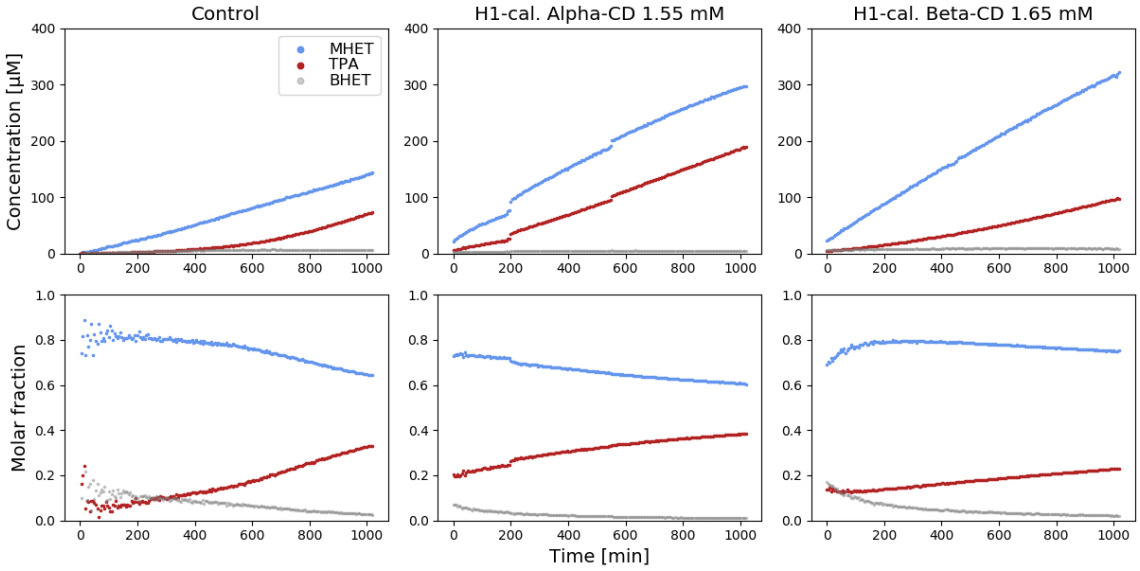

Figure 15: Estimated product concentration developments over time for enzymatic degradation of PET film (30x5 mm) by 10 μM FsC found by time-resolved ^{1}H-NMR recorded at 313 K in 25 mM sodium phosphate, 50 mM NaCl, at pD 6.5 in 96% D2O. Three experiments were performed, and the "control" panels to the left had no cyclodextrin, 1.55 mM α-CD was present for the middle panels, and 1.65 mM β-CD was present for the right panels.

The aromatic region of the time-resolved ^{1}H-NMR spectra for the β-CD experiment differed from the control and α-CD experiments. This is shown in Figure 16, where there are at least 6 peaks between the signals of the MHET-protons, spanning the region 8.05 to 8.13 ppm. These peaks have not been previously been assigned (Hellesnes et al. (2023)) and therefore these peaks were not included in the analysis of product development from the reaction. Potential causes for the unidentified peaks were discussed (See section 5.3)

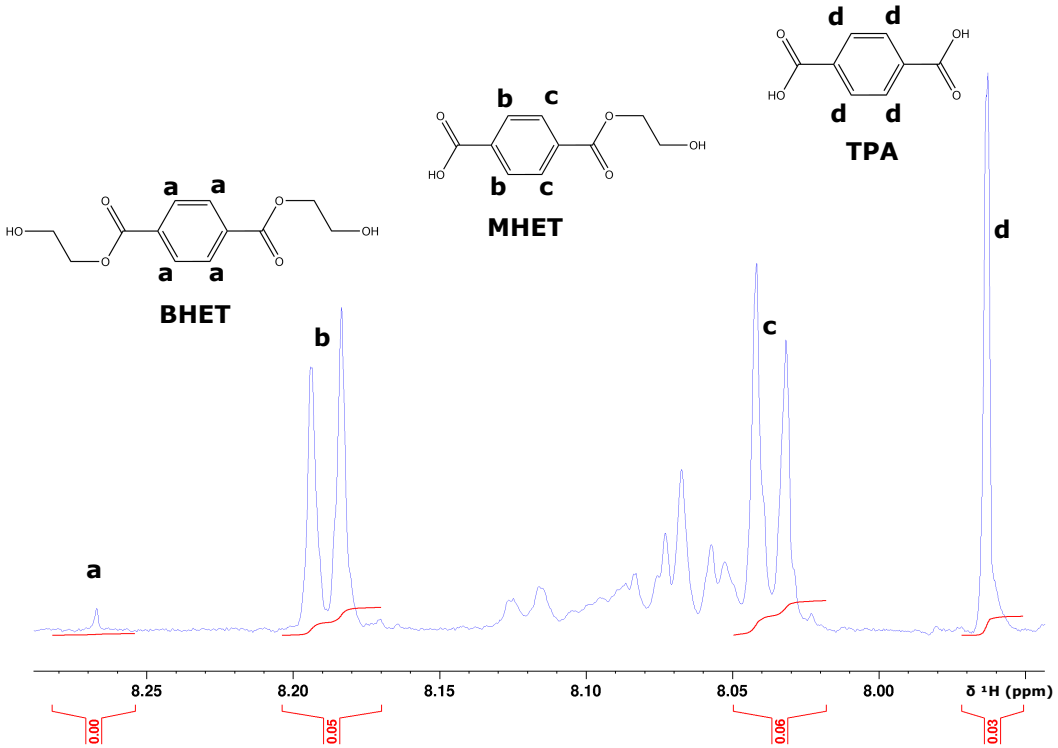

Figure 16: Part of the aromatic region in the last recorded ^{1}H-NMR spectrum in a time-resolved NMR for the enzymatic degradation of PET film (30x5 mm) with β-CD present, by 10 μM FsC in 25 mM sodium phosphate, 50 mM NaCl, at pD 6.5 in 96% D2O recorded at 313 K. Red integrals show the regions around proton peaks a (BHET, 8.27 ppm), b and c (MHET, 8.19 ppm and 8.04 ppm), and d (TPA, 7.96 ppm) used to estimate concentration developments of BHET, MHET, and TPA. Additional peaks between b and c were not assigned.

HSQC-spectra illustrating the chemical shift differences of α-CD hydrogens before and after the enzymatic degradation of PET are shown in Figure 17, where hydrogens 3 and 4 changed the most, and 6 and 5 changed the least. However, the changes were very small. The corresponding spectra for β-CD hydrogens are shown in Figure 18. H5 and H3 changed the most, followed by H6. H1 and H4 did not change notably.

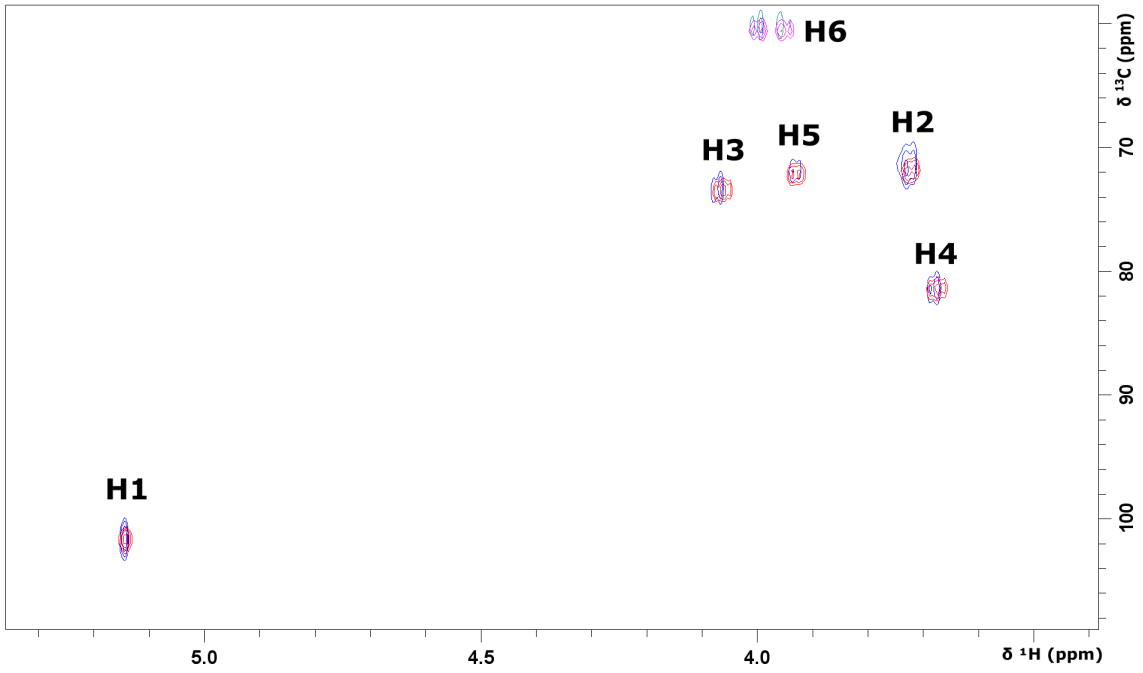

Figure 17: Overlaid HSQC-spectra of α-CD protons from before and after enzymatic degradation of a PET film (30x5 mm) by 10 μM FsC with α-CD present in 25 mM sodium phosphate, 50 mM NaCl, at pD 6.5 in 96% D2O recorded at 313 K. Blue and green signals are before, while red and pink signals are after.

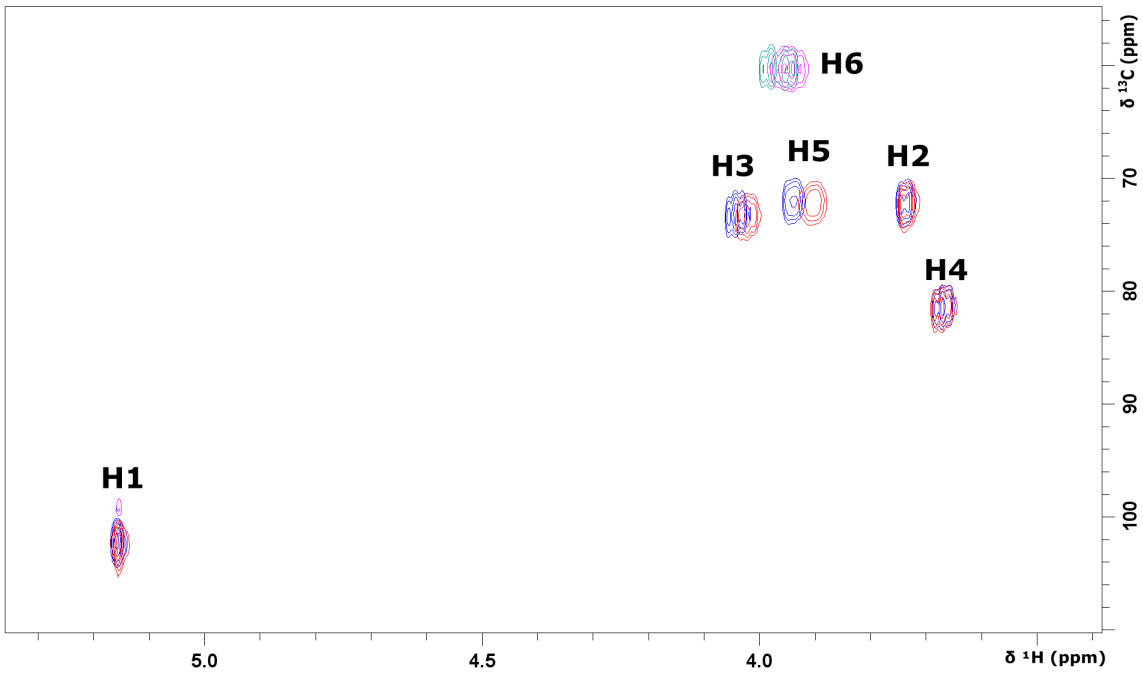

Figure 18: Overlaid HSQC-spectra of β-CD protons from before and after enzymatic degradation of a PET film (30x5 mm) by 10 μM FsC with β-CD present in 25 mM sodium phosphate, 50 mM NaCl, at pD 6.5 in 96% D2O recorded at 313 K. Blue and green signals are before, while red and pink signals are after.

5 Discussion

Possible uses of carbohydrates to improve an enzymatic recycling of PET process were investigated in this thesis. To test Hypothesis 1 from section 2, modification of glucose, cellopentaose, cellulose and β-CD was attempted to find a conjugated carbohydrate that could potentially provide an incentive to upcycle TPA, one of the monomers obtained from enzymatic degradation of PET. To test Hypotheses 2 and 3 from section 2, investigating the possibility of improving the rate of a PET-degrading enzyme, the association constants for the α-CD:TPA and β-CD:TPA inclusion complexes were estimated. Finally, investigation of the effect of CDs on enzymatic degradation of PET was done. The results described in section 4 will be discussed in this section.

5.1 Chemical modification of glucose, cellopentaose, cellulose and β-Cyclodextrin

To test Hypothesis 1 defined in section 2, and explore a method of upcycling TPA, conjugated carbohydrate molecules were attempted synthesized. Carbohydrate terephthalate esters, or even other biomolecules conjugated with plastic waste degradation products, may have potential to be part of an open cycle process where plastic waste is upcycled to make new biomaterials or biotechnological products instead of being downcycled. Using the known esterification catalyst TsCl, the carbohydrates glucose, cellopentaose, cellulose, and β-CD were chosen as candidates for modification.

For all attempts at terephthalation made here, the required evidence to confirm successful conjugation of the carbohydrate (See Figure 19) is an HMBC correlation between the carbohydrate and TPA, for example from the H6 to the carbonyl of TPA, two different proton peaks for TPA due to the assymmetry of the coupling, or FTIR absorbance bands corresponding to an ester bond connecting TPA to the carbohydrate, for example a similar band to the C=O stretch of benzoate esters that appear at 1730-1715 cm^{-1} (Silverstein et al. (2014)). None of the results show these evidence, however as discussed below, it is evident that tosylation occurred in several cases.

The choice of methodology for these experiments was based on earlier work by Lease et al, where cellulose was esterified with fatty acids using ionic liquids to dissolve the polymer and TsCl as an activator (Lease et al. (2021)). Due to the similarities between fatty acids and TPA (bulky amphiphatic carboxylic acid), it was hypothesized that the methodology could also work for TPA. However, key changes in the protocol were introduced. First, BMIMCl was chosen as the ionic liquid for reactions because of its ability to dissolve cellulose, and BMIMOAc was avoided because acetylation is known to occur (Zweckmair et al. (2015)). Second, the magnetic agate mortar and pestle described (Lease et al. (2021)) was substituted with a common magnetic stirrer for all experiments. It is likely that the increased shear would lead to more reactivity (Tan and Friščić (2018)). Third, Soxhlet-extraction was abandoned for simpler cleaning procedures, like precipitation, washing and filtering. Fourth, precipitation was done with acetone (Lease et al. (2021)), but ethanol was also used in some experiments described in section 3.2, which is common procedure (Heinze et al. (2006)).

5.1.1 Tosylation of glucose in pyridine

Reaction 1 (Table 3) was done to investigate if it was possible to see evidence of tosylation on NMR. This would confirm the first step of Path I described in Figure 4. Glucose was chosen as the simplest model system of cellulose, having the advantage of being fully soluble in pyridine.

Even though 6-tosylation was attempted by following a procedure reporting only that, the crowded region containing glucose signals makes it difficult to exclude the possibility of tosylation in other parts of the glucose molecule.

From the spectrum shown in Figure 8, the number of glucose signals suggest that other reactions took place. The spectrum shows four different signals for H6, labelled a, b, c, and d.

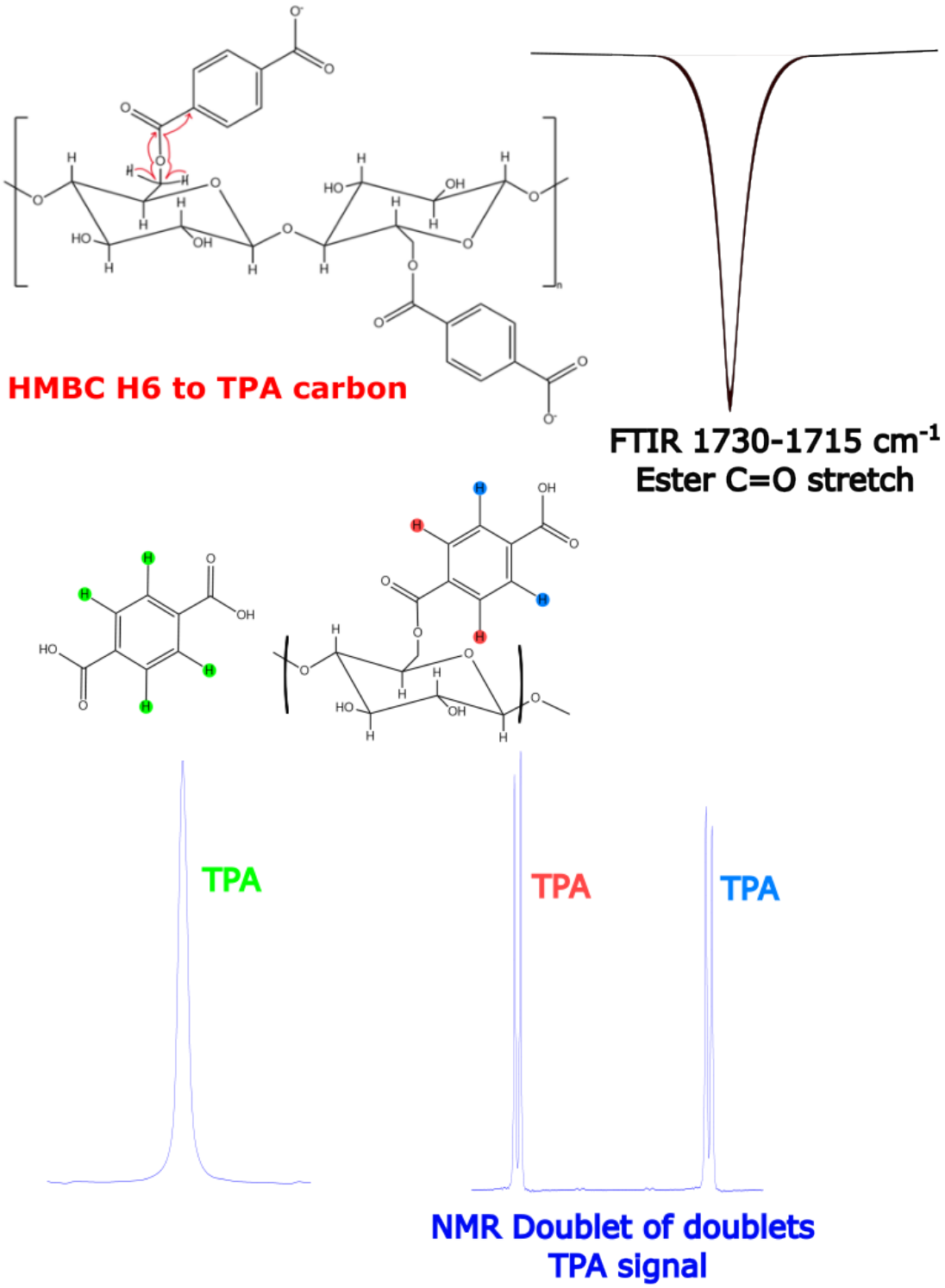

Figure 19: The required evidence for conjugation. HMBC correlation between for example H6 of a carbohydrate and one of the carbons of TPA would indicate covalent bonds between the two molecules. FTIR absorption bands for ester C=O stretch at 1730 to 1715 cm^{-1} would indicate successful esterification of TPA. Splitting of the TPA singlet to a doublet of doublets upon conjugation would indicate formation of a carbohydrate terephthalate ester.

Signal a from the figure seemed to correspond to that of H6 in β-D-glucose, with ^{13}C-shift 62 ppm (Silverstein et al. (2014)). CH_2 attached to OH in aliphatic compounds commonly have chemical shift of around 3.4 ppm, which is lower than the observed shift 3.7 ppm in Figure 8. H6 are indeed not part of an aliphatic molecule, so it makes sense that the shift is higher.

Signal b was identified as tosylated glucose by comparison with spectra of other tosylated glucans (Heinze et al. (2006)), consistent with signal b from the bottom panel of Figure 8.

Signal c showed HMBC correlation to pyridine signals in Figure A.1, suggesting that a side reaction had occurred.

A possible explanation for signal d can be chlorination, often seen in trace amounts when using TsCl for modification of cellulose, where the carbon shift of C6 is 44 ppm (Gao et al. (2018)), the same as seen in Figure 8. This suggests chlorination occurred during tosylation of glucose.

A HMBC correlation to an anomeric proton could also be seen for pyridine (Figure A.1), either suggesting two side reactions between pyridine and glucose, or reaction to a site that correlates with both C1 and C6. In Figure A.2, side reactions of pyridine with C6 and C1 of glucose were supported by the presence of signals from compounds i, ii, and iii. For Reaction 1, Figure 8 showed presence of pyridine, acetone, and three different tosyl signals, suggesting purification was insufficiently done. Ideally, the product should have been reprecipitated, and purified by Soxhlet-extraction (Heinze et al. (2006)).

5.1.2 Terephthalation of glucose in pyridine

With evidence of tosylation of glucose, Reaction 2 (Table 3) was attempted, as described in section 3.2.2. There were problems with precipitation. TPA was more difficult to dissolve in pyridine than glucose, which may have led to low concentrations of TPA, making conjugation unlikely, as can be inferred from Figure 4. As the pyridine was mixed with TPA and TsCl, there was formed a white, viscous mixture.

Reaction 2 showed only evidence of reaction on C6 as seen by signal b in the top panel of Figure B.1. The chemical shifts of this signal (4.46 ppm, 64 ppm) were different than signal b in the bottom panel of Figure 8 from the tosylation of glucose (4.35 ppm, 69.5 ppm).

The chemical shifts of signal b from the Figure B.1 were not seen in Figure 8, excluding tosylation, pyridination, and chlorination. This may indicate successful terephthalation, but more evidence is needed.

A cellulose oleate ester was reported with ^{13}C shift of C6 of 65.24 ppm (Lease et al. (2021)), close to the 64 ppm seen in Figure B.1. This makes terephthalation plausible for Reaction 2

The suggested background (Path II, Figure 4) for the reactivity of TsCl in esterification of acids to carbohydrates is intermediately formed acyl chlorides and mixed anhydrides, and these need time to form significant concentrations (Heinze et al. (2006)). The mixture of TPA and TsCl in pyridine could perhaps have reacted for example 30-45 minutes before addition to glucose to increase the reactivity.

5.1.3 Terephthalation of glucose in BMIMCl

Reaction 3 (Table 3) as means of in situ activation of TPA was attempted. Even though ionic liquids like BMIMCl are not necessary for the reaction, this was done to have a basis for understanding the reaction with cellulose, in which the polysaccharide needs to be dissolved in BMIMCl.

As described in section 3.2.3, acetone was added to cause precipitation to separate different compounds. This was done because it caused precipitation previously, so it was assumed to help separate the product. Although it did not cause precipitation, it is likely that some compounds were extracted from the BMIMCl phase, as the color of the acetone fraction changed slightly.

Addition of ethanol led to a homogenous mixture with the BMIMCl-phase. This is why it was chosen to evaporate the solvents, and try to analyze the mixtures anyway. Water was found to cause precipitation of both the BMIMCl fraction and the acetone fraction.

After examination of HSQC spectra from the four fractions from terephthalation of glucose in BMIMCl, the water fraction from the BMIMCl-phase was the only one found to contain glucose signals. This part of the spectrum was shown in Figure C.1, where the number of sugar-like signals exceeded the expected number of glucose signals for α-H1, β-H1, and H2 through H6.

This could suggest a reaction taking place that results in other versions of glucose hydrogens. C6 modification seems unlikely here, given that only one version of the H6 signal was present. Reaction at C2, C3 or C4, was not ruled out. The sugar-region of the spectrum, however, is too crowded by impurities to suggest a specific reaction. All other compounds in the mixture seemed to exist in just one version, leaving no clue for what could have reacted.

To improve the purity of the product for this experiment, ethanol as the antisolvent should have been used first, according to a successful procedure for extracting pure glucose from ionic liquids (Hassan et al. (2013)). In this procedure, the temperature difference between ethanol and the ionic liquid should be as large as possible, and the ethanol:ionic liquid ratio is suggested to be high. Much more ethanol should therefore have been added. Room temperature, or even refrigerated ethanol added to the hot ionic liquid mixture could have improved the precipitation of glucose and eventual products. It is reasonable to assume that a terephthalated glucose molecule would also be little soluble in an ethanol-ionic liquid mixture. Subsequent filtering would then recover the glucose and its potential derivatives.

It is not clear what would happen to unreacted substances if the ethanol antisolvent method had been done properly. If the temperature of ethanol is kept low and excess of ethanol relative to ionic liquid is high, it is possible that TPA would precipitate along with glucose. TPA is reported as poorly soluble in alcohols, and also insoluble in BMIMCl at 25 ℃(Matuszek et al. (2020)). Precipitation of TPA would require another purification step.

TsCl is not reported to precipitate in BMIMCl and pyridine mixture with excess of ethanol (Gericke et al. (2012)), and would likely in the antisolvent method (Hassan et al. (2013)) remain dissolved. TsCl would further be separated from glucose, modified glucose, and TPA.

Pyridine could easily be evaporated, and the difference in water solubilities for glucose and TPA could be exploited for separation of these.

5.1.4 Subsequent tosylation and terephthalation of cellopentaose in BMIMCl

The tosylation and terephthalation of cellopentaose was done to explore possible changes in reactivity between a monosaccharide and an oligosaccharide, with the sugar still being soluble enough for NMR analysis. The procedure is described in section 3.2.4. Water was used to separate the compounds after learning ethanol and acetone was insufficient from terephthalation of glucose done in BMIMCl (Section 5.1.3).

With reagents cellopentaose and TsCl dissolved in BMIMCl, tosylation and chlorination of cellopentaose could have occurred. Adding TPA could have led to terephthalation of cellopentaose.

The HSQC spectrum of the water fraction of the BMIMCl phase in Figure D.1 in the appendix, showed very weak and obstructed sugar signals, almost indistinguishable from noise. Only one weak signal for H6 was present, but chemical shifts (3.5 ppm, 60 ppm) indicate that it is the normal CH_2-OH from cellopentaose. This in itself may exclude 6-terephthalation, but along with the absence of a TPA signal in the same spectrum, shown in the bottom panel of Figure D.1, it seems very unlikely terephthalation occurred. Also, signals d and e from Figure D.1 seem like only one version of tosyl protons is present, indicating unsuccessful tosylation as well.

5.1.5 Tosylation and terephthalation of cellulose in BMIMCl with pyridine as co-solvent

Cellulose terephthalate could have useful properties, providing incentive for upcycling of TPA, as explained in section 1.3.2. To test Hypothesis 1 defined in section 2, and attempt synthesis of CTP, terephthalation of cellulose was attempted in BMIMCl, as described in section 3.2.5. The results from this experiment were FTIR spectra (Figure E.1), with band assignment primarily done by comparison with common polysaccharide absorbance bands.

During dissolution of cellulose in BMIMCl, the viscocity of the liquid increased. It is likely that the magnetic stirrer could not mix the liquid well, leading to an inhomogenous mixture. This may have limited the reactivity by reactants not coming in contact.

Tosylation of glucose was described in section 4.1, leading to expectations of successful tosylation of cellulose, with all the same reactants being present. Terephthalation of cellulose was also possible here, and evidence of chlorination of glucose may suggest the possibility of chlorination also occurring for cellulose.

As mentioned in Figure 19, an ester bond visible on FTIR spectrum would be sufficient evidence for successful conjugation. The ester C=O stretch was assigned at 1731 cm^{-1} by Lease et al. in the synthesis of a cellulose oleate ester (Lease et al. (2021)). Benzoate ester C=O stretches are generally found in the 1730 to 1715 cm^{-1} region (Silverstein et al. (2014)). The absence of any absorption band in the range 1730-1715 cm^{-1} in Figure E.1 indicated that the reaction between cellulose and TPA did not occur. Another indication of unsuccessful reaction was the band at 1671 cm^{-1}, which may be assigned to the TPA C=O stretch, seen at 1693 cm^{-1} (Pretsch et al. (2013)).

The TOSC FTIR spectrum in Figure E.1 showed absorption at 1109 cm^{-1}, and the terephthalated cellulose showed a band 1110 cm^{-1}. Aromatic esters of primary alcohols show absorption near 1111 cm^{-1} from O-C-C (alcohol carbon–oxygen stretch)(Silverstein et al. (2014)). However, sugar ring antisymmetric stretch is claimed to cause absorption bands around 1110 cm^{-1} (Heinze et al. (2006)). With the absence of the ester carbonyl band (1730-1715 cm^{-1}), it is likely that the bands seen here are caused by sugar rings of cellulose.

In the top panel in Figure E.1, TOSC absorbance bands at 1371 and 1163 cm^{-1} may be assigned to the asymmetric and symmetric stretch of the S=O bond, respectively (Silverstein et al. (2014)). The characteristic tosylation bands of O-SO_2-R have been reported in literature at 1350 and 1175 cm^{-1} (Mocanu et al. (1996)). The antisymmetric S=O stretch of tosylated cellulose has also been assigned as 1390 cm^{-1} (Granström et al. (2008)). The observed 1371 cm^{-1} band is close to 1367 cm^{-1} reported prievously (Koschella and Heinze (2003)). The FTIR spectrum for TOSC shows a band at 1371 cm^{-1} that is not assigned to anything else, while terephthalated cellulose has no bands close to this, seen in Figure E.1. The bands closest to 1175 cm^{-1} are 1163 and 1161 cm^{-1} for TOSC and terephthalated cellulose, respectively. The two bands also fit with C-O-C antisymmetric stretch for polysaccharides, commonly seen in the range 1162-1125 cm^{-1} (Heinze et al. (2006)). The two bands so close are present in both spectra shown in figure E.1, and may be caused by the same vibration, which is more likely from the cellulose than from the tosyl group.

Chlorination of cellulose was not ruled out from spectra in Figure E.1. The wide frequency range for CH_2-Cl wagging, 1500 to 1300 cm^{-1} can be confused with other CH_2 vibrations in the same region (Heinze et al. (2006)). Chlorination has been reported previously in cellulose, with a C-Cl band at 753 cm^{-1} (Gao et al. (2018)). Another source reports the C-Cl band at around 700 cm^{-1} (Mocanu et al. (1996)). A band is seen at 753 cm^{-1} in the FTIR spectrum for TOSC in Figure E.1 (Top). In the spectrum for terephthalated cellulose (Figure E.1, bottom), strong bands are seen at 780 and 726 cm^{-1}, which may correspond to chlorination.

Rapid phase separation of the gel like material after tosylation may have caused compounds present in the mixture to become trapped by the quick and inhomogenous formation of a solid. FTIR band at 1635 cm^{-1} is commonly known to occur when water is adsorbed to the sample (Heinze et al. (2006)), confirming suspicions that the sample was impure. Although water was not added to the reaction, water may have been present in the ethanol, or the BMIMCl, which is known to be hygroscopic (Takada and Kadokawa (2022)). Precipitation should have been done more carefully

to get a purer product.

To improve the reactivity, TPA and TsCl should perhaps have been mixed before reacting with TOSC. This would promote Path II in Figure 4. Another possibility is to have done the reaction in one step, without the confirmation of tosylation. Mixing cellulose and TPA in BMIMCl, and then adding TsCl had been more similar to Lease et al., where cellulose and oleate was mixed in BMIMOAc, and TsCl was added after 1 hour (Lease et al. (2021)). It is also possible that the changes in the procedure from Lease et al. mentioned at the start of section 5 may have been impactful for the failed synthesis of CTP.

5.1.6 Tosylation of β-Cyclodextrin

Similarly with cellulose, a conjugated β-CD could have interesting properties as described in section 1.3.3. Characterization of the tosylated product was important at this point, as the FTIR spectrum of TOSC was not entirely conclusive regarding the tosylation of cellulose. To test if the first step in Path I from Figure 4 occurred, analysis of the tosylated β-CD was done before terephthalation, discussed in section 5.1.7. Reaction 6 (Table 3) was performed as described in section 3.2.6.

The procedure had previously reported good results for monotosylation at C6 (Melton and Slessor (1971)), so tosylation was expected. As shown in Figure 9, an additional H6 signal, b (4.2 ppm, 70 ppm), was observed, corresponding with chemical shift changes consistent with tosylation.

As with previous reactions, chlorination was also considered to be possible here. Indication of chlorination would be the additional H6 peaks at around 3.85 ppm and 44 ppm seen in Figure 8, but they were not observed in Reaction 6 (Figure 9).

The same solvent (pyridine) was employed for Reaction 6 as for Reaction 1. In Reaction 1, unwanted side reactions between pyridine and glucose was shown in Figures A.1 and A.2, as discussed in section 5.1.1. Side reactions with pyridine were also considered possible for Reaction 6. From Figure 9, absence of signal near (4.8 ppm 62 ppm) indicated no pyridine side reactions for Reaction 6.

With no smell of pyridine after evaporation, no further purification was done before terephthalation was attempted (Reaction 7). It was clear from Figure F.1 that pyridine was still present (purification was discussed for Reaction 6 and 7 together in section 5.1.7).

5.1.7 NaOH-activated terephthalation of tosylated β-Cyclodextrin

The last test of Hypothesis 1 (section 2) consisted in attempting to synthesize a β-CD terephthalate ester. Reaction 7 (Table 3) was done by continuing with the tosylated β-CD, as the first step of Path I (Figure 4) was confirmed to occur in Reaction 6.

NaOH was used in this experiment, as described in section 3.2.7, to try to activate TPA by deprotonation, as no evidence of Path II from Figure 4 was seen up to this point. The idea was that the negatively charged oxygen would be more nucleophilic, and attack the C6 of β-CD to substitute the tosyl group. It was hypothesized that the strong base NaOH would accomplish this deprotonation/activation to a larger extent than pyridine.

As described in section 4.1.7, a precipitate formed for Reaction 7. TPA was likely present in the precipitate, as the NMR signal from the freeze-dried solids from the supernatant after centrifugation (dissolved in D_2O) gave no TPA signal. In contrary, the precipitate dissolved in DMSO-d_6 gave a strong signal for TPA, signal d in Figure 10.

Results from DOSY shown in Table G.1 also confirmed the tosylation of β-CD because of the similar values reported for D between β-CD protons and tosyl group protons. The D for TPA (4.2 $\times 10^{-11}$ m^2/s) was just under double of the values reported by β-CD protons.

Comparing the value for TPA with the values for free TsCl, (5.7, 6.7, and 8.3 $\times 10^{-11}$ m^2/s), the similarly sized molecules were expected to have more similar diffusion coefficients. One explanation

for the seemingly low D for TPA can be that inclusion complex formation with β-CD can affect the observed D. In DOSY, for a host:guest relationship, the measured D is a weighted average of the free and bound diffusion coefficients (Cohen et al. (2005)). The values seen for TsCl may also be subjected to inclusion complex effects.

One explanation for the absence of β-CD terephthalate could be the presence of water. As NaOH and TPA were mixed in aqueous solution before addition of the tosylated CD, water could have contributed to increasing the hydrolysis rate of the ester bonds, possibly outcompeting their rate of formation. This, along with prolonged reaction time has been reported to lower the degree of substitution in other esterification reactions with acyl chlorides and cellulose (Freire et al. (2006)).

From Figure 10, signals a, b, and c from pyridine, d from TPA, and g and h from TsCl suggest improving purification may be necessary, although it was not the primary focus in this thesis. There were still pyridine signals in Figures F.1 and 10, despite no pyridine smell from the sample. Further evaporation at reduced pressure at 40 ℃before freeze-drying could have increased the purity of the sample. Also, if the tosylated β-CD had poor water solubility, more washing in larger amounts of water could have helped remove unreacted TsCl, and possibly TPA despite its poor water solubility. And ideally, a Soxhlet extraction could have improved removal of unreacted compounds.

The results from Reaction 7 included none of the required evidence for successful conjugation of TPA to β-CD introduced in Figure 19. This concluded the testing of Hypothesis 1 from section 2. Hypothesis 1 was rejected.

5.2 Cyclodextrin:Terephthalic acid inclusion complex

Inclusion complexes between CDs and PET degradation products were hypothesized to improve the enzymatic degradation (Hypothesis 3, section 2). The proposed mechanism for this was that CDs would temporarily and reversibly form inclusion complexes with the degradation products in the reactor, making the aromatic compounds BHET, MHET, and TPA unavailable for the enzyme. This would reduce the available concentration of inhibitory degradation products. The observed effect of this would be reduced product inhibition and increased degradation rate.

It was important to characterize the complexation between CDs and PET degradation products (Equation 1) to determine the feasibility of employing CDs to increase the enzymatic degradation rate of PET. For this, TPA was used as a model substrate, and Hypothesis 2 from section 2 was defined. K_a (Equation 2)indicates the interaction strength between the two molecules, and can provide insight about the effectiveness of the inclusion complex. A high value for K_a would suggest that CDs bind TPA tightly, and would keep TPA away from the enzyme. A low value for K_a would indicate weak interaction, meaning TPA would be more likely to inhibit the enzyme. Thus, determination of K_a would provide foundation to determine the feasibility of using CDs to reduce product inhibition for the enzymatic degradation of PET by FsC.

Hypothesis 2 was tested by NMR titration to determine K_a, as described in section 3.3.

Considering the structure of CDs shown in figure 5, H5 and H3 were expected to be the most potent reporters for association with TPA for both α-CD and β-CD because they point in towards the cavity of the CDs.

5.2.1 Determination of association constant for the inclusion complex β-CD:TPA

The feasibility of using β-CD to increase the rate of enzymatic degradation was investigated by determining K_a for the β-CD:TPA inclusion complex. Hypothesis 2, TPA forms inclusion complexes with CDs, from section 2 was tested here. NMR titration was the chosen method, measuring $\Delta\delta^1$H for β-CD protons with different concentrations of TPA. The idea was to assess, or potentially exclude, using β-CD to increase the PET degradation rate of FsC. It was also important to identify which protons that could report the most reliable estimate for K_a.

H5 was chosen because its chemical shift was most responsive to the increasing concentration of TPA of all β-CD protons (Figure 12). The high values for K_d and unrealistic values for $\Delta\delta^1 H_{max}$ reported for H1, H3, and H6 in Table 4 made these protons unsuitable for describing association with TPA. Only using H5 as a reporter has been done previously, where an NMR titration showed that phthalic acid esters formed inclusion complexes with β-CD (Murai et al. (1998)). The same study saw stability constants for the host:guest complex increasing with alkyl chain length for phthalic acid esters of small alkanes. Their results suggest that β-CD accomodates larger and more hydrophobic benzene derivatives better than the smaller ones, such as TPA. This led to expectations of α-CD being more strongly associated with TPA than β-CD and TPA because of the smaller size of α-CD being a tighter fit for TPA.

$\Delta\delta^1 H_{max}$ is the chemical shift difference of CD protons at saturation of TPA. The concentrations of TPA used in this experiment (Table 1) were likely far from saturation because of poor solubility of TPA. Good estimations of K_a and K_d require full saturation of β-CD with TPA, which was likely not reached due to low solubility of TPA.

In section 4.2.1, K_a was estimated to be 16 M^{-1}, and K_d was estimated as 63 mM for the β-CD:TPA inclusion complex based on H5 as reporter. Jackknife error estimation (Efron and Stein (1981)) was done for H5 by systematically leaving one point out of the data set when calculating K_d, then taking the average of all the estimates, and calculating a standard deviation. This led to the estimate for K_d as 57±20 mM. Jackknifing was chosen because the highest concentration points in Figure 12 appeared to have a strong influence of the fit of the two state exchange model to the data. The large error (35%) leaves uncertainty of the estimate, but the interaction can still be interpreted qualitatively as very weak.

5.2.2 Determination of association constant for the inclusion complex α-CD:TPA

The feasibility of using α-CD to increase the rate of enzymatic degradation was investigated by determining K_a for the α-CD:TPA inclusion complex. By doing this, the strength of interaction between α-CD and TPA could reveal whether α-CD could be used to increase the FsC-catalyzed PET degradation rate by binding BHET, MHET, and TPA to reduce product inhibition of the enzyme. Hypothesis 2, TPA forms inclusion complexes with CDs, from section 2 was tested by NMR titration according to section 3.3.2, measuring $\Delta\delta^1$H for α-CD protons with different concentrations of TPA. It was also important to identify which protons that could report the most reliable estimate for K_a.

It was also here important to establish which protons could respond appropriately to change in concentration of TPA. H3 and H5 were almost equally responsive in terms of euclidean distances ($\Delta\delta_{ppm}$) from the pure α-CD sample, as seen in Figure 14. In Figure 13, however, the chemical shift of α-CD H3 was seen to decrease, while the opposite was observed for H5 (increasing chemical shifts) as a result of increasing the concentration of TPA. The increasing chemical shift observed for H5 of α-CD as a response to increasing concentration of TPA was the opposite of observations for H5 in β-CD. The different responses for H5 of α-CD and β-CD could originate from differences in orientation of TPA inside the CD cavity.

$\Delta\delta^1 H_{max}$ from Equation 3 is the chemical shift difference of CD protons at saturation of TPA. The concentrations of TPA used in this experiment (Table 2) were likely far from saturation, even further than from the corresponding β-CD experiment. Good estimations of K_a and K_d require full saturation of α-CD with TPA, which was likely not reached because of poor solubility of TPA.

In section 4.2.2, K_a was determined to 43 M^{-1}, and K_d was determined to 23 mM. For comparison with β-CD, jackknifing (Efron and Stein (1981)) was also done for α-CD. For the α-CD:TPA inclusion complex, the highest concentration points in Figure 14 did not appear as influential on the fit of the two state model as $\Delta\delta^1$H for the highest concentration of TPA for β-CD protons in Figure 12. The procedure for jackknifing was described in section 5.2.1. Doing jackknife error estimation on α-CD H5 gave the estimate for K_d 23±7 mM. The error was also high here, at 30%, and the interaction between α-CD and TPA is considered weak.

The results discussed in section 5.2.2 showed that β-CD and α-CD formed inclusion complexes

with TPA. Hypothesis 2 from section 2 was therefore confirmed. However, values for K_a for both CD:TPA inclusion complexes suggested that the interactions were weak. The feasibility of using CDs to

5.3 Investigation of the effect of cyclodextrins on PET degradation rate of a wild-type FsC using time-resolved NMR

To test Hypothesis 3 from section 2, the effect of the presence of CDs on PET degradation rate for FsC was investigated using a continuous assay based on time-resolved NMR (Hellesnes et al. (2023)). Three corresponding degradation experiments were done with FsC and PET, without, with α-CD, and with β-CD, as described in section 3.4.2. The enzymatic degradation reactions were described in Figure 6.

Based on final concentrations of BHET, MHET, and TPA, apparent degradation rates, were calculated by the secant method (Kari et al. (2019)). The apparent degradation rates estimated in section 4.3 revealed that the presence of either CD resulted in around two times higher concentrations of MHET than for the control. Concentrations of TPA were three times higher for α-CD than for the control. BHET concentrations were overall low, but highest for β-CD, possibly indicating the faster hydrolysis of BHET than PET. Overall, presence of CDs led to higher concentrations of PET degradation products.

An explanation for the higher degradation rates of PET by FsC during the presence of CDs may be that the degradation products, BHET, MHET, and TPA, can to a larger extent form inclusion complexes with CDs instead of occupying the FsC and preventing degradation of PET. Presence of CDs would promote continued degradation of PET, leading to higher concentrations of degradation products, which was in fact observed.

The conditions used for the investigation of the effect of CDs on PET degradation rate for FsC (10 μM FsC, 25 mM sodium phosphate buffer containing 50 mM NaCl, pD 6.5, low crystallinity PET film, 40 ℃) were the same as in (Hellesnes et al. (2023)). The degradation by wild-type FsC saw concentration of MHET peaking at over 800 μM after around 400 minutes, and was then reduced to around 700 μM towards the end of the experiment, and product distribution was around 0% BHET, 70% MHET, and 30% TPA (Hellesnes et al. (2023)). The reported value for concentation of MHET is around three times as high as the highest MHET concentrations for α-CD and β-CD present, and over four times higher than for the control sample observed in this thesis. Product distributions shown in Figure 15 were similar to that seen previously at pD 6.5 (Hellesnes et al. (2023)). The higher activity seen in (Hellesnes et al. (2023)) despite similar conditions may be explained by loss of activity for FsC during storage.

The basis for calculation of apparent rates was the assumption of linearity of the product concentration developments. This was done to give a simple measure used to compare the three different conditions for enzymatic degradation of PET. By visual inspection alone, the TPA curve for the control in Figure 15, is seen to be non-linear, but for the purpose of comparing the three experiments, the linearity was deemed sufficient. Kinetic studies to find inverse Michaelis-Menten parameters are needed to characterize the effect of CDs on the rate of FsC-catalyzed degradation of PET to a deeper extent (Pirillo et al. (2021)).

From Figure 16, NMR signals of varying intensities can be seen in the region 8.05 to 8.13 ppm. These peaks have not been assigned previously (Hellesnes et al. (2023)), but they could possibly originate from soluble PET oligomers. Deeper investigations of these signals would be interesting, to find out if they are in fact PET oligomers. Since the signals could originate from larger PET degradation products, the enzymatic degradation experiment with β-CD present could have more degradation of PET occurring than what is reported from developments of BHET, MHET, and TPA concentrations.

A relationship between the structure of the CD and the product distribution may be inferred. α-CD, because of its smaller size (six glucose units) may more easily form inclusion complexes with the smaller molecules MHET and TPA. Whereas the larger β-CD (seven glucose units) may

accommodate the larger degradation products like BHET and possibly also oligomers. Because BHET and possibly larger PET oligomers would be tighter associated with β-CD than α-CD, BHET and oligomers would be less accessible to the enzyme for further degradation, leading to lower fractions of TPA for β-CD than for α-CD. Presence of α-CD could accommodate the smaller products, leaving larger fragments free to be degraded fully by the enzyme, leading to larger fraction of TPA produced than for β-CD. The absence of CDs might give an intermediate distribution of products. A deeper investigation of this relationship with different enzyme:CD ratios would be interesting.

The time-resolved ^{1}H-NMR method to monitor product concentrations of a degradation reaction has been employed previously (Hellesnes et al. (2023)). The recording of developments of all products simultaneously and continuously is powerful, though specific NMR-related phenomena can affect measurements. For example, the insoluble PET film present in the NMR tube may cause line broadening by disturbing the homogeniety of the magnetic field (Hellesnes et al. (2023)). As a complement to the NMR monitored enzymatic degradation of PET, a discontinuous UV absorbance assay with manual sampling could have been done. This would either confirm the results or lead to questioning of the method, as UV assays are well established methods for measuring enzymatic activity (Pirillo et al. (2021)).

The degradation of PET was seen to increase by presence of CDs. The suggested explanation was that parts of the aromatic degradation products were temporarily removed from the solution, making them unavailable for the FsC, ultimately reducing product inhibition. It has been shown for another cutinase, TfCut2, that an ultrafiltration module can reduce product inhibition (Barth, Wei et al. (2015)). A setup is described where a pump pushes reaction media through a filter that small molecules (MHET, BHET, TPA) pass, while larger PET fragments and enzymes are returned to the reactor (Barth, Wei et al. (2015)). The ultrafiltration module would physically remove the deagradation products from the reaction mixture, whereas CDs in the solution would form inclusion complexes with the PET degradation products, making them less likely to prevent the enzyme from degrading PET. The ultrafiltration module (Barth, Wei et al. (2015)) and presence of CDs are ways to lower the effect of product inhibition for the enzymatic degradation of PET. However, in the ultrafiltration module, weight loss of PET films used decreased only by 6% over 24 hours (Barth, Wei et al. (2015)), confirming that enzymes need higher rates to operate efficient enzymatic recycling of PET on a large scale.

In the investigation of the effect of CDs on the FsC-catalyzed degradation of PET, presence of CDs doubled the concentration of MHET compared to the control, presence of α-CD tripled concentration of TPA compared to the control, and unknown NMR signals at 8.05 to 8.13 ppm appeared in the presence of β-CD. From these findings, presence of CDs seemed to increase degradation rate of PET overall, and the proposed explanation for the increase in rate was that CDs form inclusion complexes with the PET degradation products, which prevented accumulation of inhibitory products, and promoted further degradation of PET. Hypothesis 3 from section 2 was confirmed based on the discussion in this section.

Although the findings of increased degradation rate of PET with CDs present are interesting, the potential of industrial adoption of the utilization of CDs to increase the rate of enzymatic PET degradation may be limited. In this thesis, mM concentrations of cyclodextrins were present, and μM concentrations of PET degradation products were observed. Upscaling this might lead to requirements of unrealistic amounts of CDs compared to the amount of PET degraded. Despite this, the potential of carbohydrates to improve enzymatic degradation of PET may still be high.

6 Future research

6.1 Chemical modification of glucans using PET degradation products

During attempts at conjugating glucans in attempted upcycling of TPA, Path II from Figure 4 was not observed. The in situ activation of a carboxylic acid using TsCl was documented elsewhere using time-resolved ^{1}H-NMR, by following developments of concentrations for TsCl, carboxylic

acid, acyl chloride, anhydride, and mixed anhydride (Heinze et al. (2006)). Confirmation of Path II being applicable for TPA is suggested before attempting further reactions.

By replacing TPA with acetic acid, the same procedure for synthesis of CTP described in section 3.3.5 could have been tested to get insight in whether TPA had low reactivity, or if the procedure was lacking. This would exploit the known reactivity of acetate to cellulose (Xu et al. (2011)).

As described in the introduction of section 5, the procedure from Lease et al. was modified on four key points, choice of ionic liquid, not using magnetic mortar, not using Soxhlet extraction, and precipitation agent. It would be interesting to test the synthesis of CTP using the magnetic mortar, which may be of highest influence of the four changes. As good results for synthesis of cellulose oleate was seen (Lease et al. (2021)), CTP may be synthesized under more equal conditions.

It has also been seen in this thesis that presence of cyclodextrins can modify the degradation product distributions for FsC degradation of PET. Dominance of MHET as a degradation product led to the idea of a mixed cyclodextrin terephthalate MHET ester synthesized from the mixture in the degradation vessel after extracting the FsC. The properties of a CD-TPA-MHET mixed ester could resemble those described for β-CD terephthalate ester in section 1.3.3. With higher degree of substitution, perhaps the aromatic groups from conjugated MHET, or even PET oligomers, could extend the CD cavity or better accommodate longer molecules.

6.2 Inclusion complexes between cyclodextrins and PET degradation products

In this thesis K_a and K_d were determined for the α-CD:TPA and β-CD:TPA inclusion complexes. As inferred from the structures of TPA, MHET, and BHET, they interact with α-CD and β-CD differently. It would be interesting to estimate K_a and K_d for the CD:MHET and CD:BHET inclusion complexes as well.

6.3 Investigation of the effect of cyclodextrins on PET degradation of a wild-type FsC

To validate the results obtained from time-resolved ^{1}H-NMR of the degradation of PET by FsC, a UV absorbance assay could be done. The discontinuous absorbance assay (Pirillo et al. (2021)) could have been done in parallel with a new, continuous absorbance assay (Thomsen et al. (2023)) to learn more about the new technique.

Doing the UV absorbance assay would allow determination of inverse Michaelis-Menten kinetic parameters for the FsC degradation of PET (Pirillo et al. (2021)).

Further work on biochemical characterization of the FsC could also include confirming that the enzyme is prone to product inhibition of especially MHET and BHET. This has already been done for another PET hydrolyzing cutinase, the TfCut2 (Barth, Oeser et al. (2015)).

As seen in Figure 16, and discussed in section 5.3, unidentified peaks in the region 8.05 to 8.13 ppm were observed. These were hypothesized to be soluble PET oligomers, but no efforts were made to characterize them. For the continuation of research on enzymatic degradation of PET, it is recommended that these peaks are characterized. To accomplish this, different compounds would need to be separated and characterized, perhaps in a UHPLC-MS/MS method (Rathod et al. (2019)). To aid the characterization, a library of PET oligomers of known structures could be analyzed for comparison. Adsorption of compounds to the PET film was also suggested, and this could be investigated by removing the film before recording another ^{1}H-NMR scan, where all the unidentified signals would be absent if they were caused by adsorption to the PET film. NMR is a useful technique to study the enzymatic degradation of PET, and establishing a complete framework for other researchers could benefit the overall aim of this thesis, improving an idealized enzymatic degradation of PET process using carbohydrates.

The different degradation product distributions shown in Figure 15 show that the distributions are different for no CD, α-CD, and β-CD in similar concentrations. It would be interesting to investigate if the degradation product distributions are tunable from adjusting the concentrations of CDs, and even in different ratios. Varying concentrations and ratios could also have an effect on the degradation rates.

7 Conclusions

In this thesis, the potential of using carbohydrates to improve a hypothetical enzymatic degradation of PET process was investigated. To improve the process using carbohydrates, three hypotheses were made, addressing upcycling of the degradation products of PET, and increasing the rate of degradation for the PET hydrolyzing enzyme FsC.

Hypothesis 1 was that esterification of cellulose with TPA could be a feasible way to produce a new conjugated polymer, CTP, with novel properties. The soluble model carbohydrates glucose, cellopentaose, and β-CD were used to gain insight on the reaction by NMR. CTP was not observed, by absence of ester bond vibrations in an FTIR spectrum of the product from reaction with TPA and TsCl in the ionic liquid BMIMCl. This indicated that the procedure used was not a feasible way to produce CTP. Hypothesis 1 was rejected. Despite this, there may be other ways to use carbohydrates in the upcycling of PET degradation products that were not explored in this thesis.

Hypothesis 2 was that TPA forms inclusion complexes with α-CD and β-CD. NMR titrations were performed with constant concentrations of CDs and varying concentrations of TPA, leading to fitting of a two state exchange model to chemical shift perturbations, allowing determination of K_a and K_d for the α-CD:TPA and β-CD:TPA inclusion complexes, using H5 as a reporter. Association was seen to be stronger for the α-CD:TPA inclusion complex than for β-CD:TPA. Large relative errors indicate uncertainty in the method, but the qualitative take-away was that interactions were weak between the CDs and TPA. Hypothesis 2 was confirmed.

Hypothesis 3 was that cyclodextrins form inclusion complexes with PET degradation products to improve the rate of enzymatic degradation of PET, by reducing product inhibition. A time-resolved ^{1}H-NMR experiment was set up to monitor soluble degradation product concentrations over time for enzymatic degradation by FsC without CD, with α-CD, and with β-CD. The developments of degradation product concentrations were overall higher when CDs were present. Product distributions showed that α-CD promoted the smaller degradation products, while β-CD promoted the larger degradation products. MHET, the most accumulating degradation product, was produced at twice the rate when CDs were present relative to the control sample with no CD. Hypothesis 3 was confirmed. However, the real applicability of CDs in a PET degradation reactor may be unrealistic.

Although the findings in this thesis were interesting, addressing the overarching aim of the thesis, improving an idealized enzymatic degradation of PET process using carbohydrates, was of limited impact. The thesis has nonetheless delivered a foundation for further work on employing carbohydrates to improve an enzymatic degradation of PET process.

References

Alsbaiee, A. et al. (Jan. 2016). 'Rapid removal of organic micropollutants from water by a porous β-cyclodextrin polymer'. In: *Nature* 529.7585, pp. 190–194. ISSN: 1476-4687. DOI: 10.1038/nature16185. URL: https://doi.org/10.1038/nature16185.

Barth, M., Oeser, T. et al. (2015). 'Effect of hydrolysis products on the enzymatic degradation of polyethylene terephthalate nanoparticles by a polyester hydrolase from Thermobifida fusca'. In: *Biochemical Engineering Journal* 93, pp. 222–228. ISSN: 1369-703X. DOI: https://doi.org/10.1016/j.bej.2014.10.012. URL: https://www.sciencedirect.com/science/article/pii/S1369703X14002964.

Barth, M., Wei, R. et al. (2015). 'Enzymatic hydrolysis of polyethylene terephthalate films in an ultrafiltration membrane reactor'. In: *Journal of Membrane Science* 494, pp. 182–187. ISSN: 0376-7388. DOI: https://doi.org/10.1016/j.memsci.2015.07.030. URL: https://www.sciencedirect.com/science/article/pii/S0376738815300582.

Cohen, Y., Avram, L. and Frish, L. (2005). 'Diffusion NMR Spectroscopy in Supramolecular and Combinatorial Chemistry: An Old Parameter—New Insights'. In: *Angewandte Chemie International Edition* 44.4, pp. 520–554. DOI: https://doi.org/10.1002/anie.200300637. eprint: https://onlinelibrary.wiley.com/doi/pdf/10.1002/anie.200300637. URL: https://onlinelibrary.wiley.com/doi/abs/10.1002/anie.200300637.

Corcoran, P.L., Biesinger, M.C. and Grifi, M. (2009). 'Plastics and beaches: A degrading relationship'. In: *Marine Pollution Bulletin* 58.1, pp. 80–84. ISSN: 0025-326X. DOI: https://doi.org/10.1016/j.marpolbul.2008.08.022. URL: https://www.sciencedirect.com/science/article/pii/S0025326X0800430X.

Efron, B. and Stein, C. (1981). 'The Jackknife Estimate of Variance'. In: *The Annals of Statistics* 9.3, pp. 586–596. DOI: 10.1214/aos/1176345462. URL: https://doi.org/10.1214/aos/1176345462.

European Commission (2022). *EU Strategy for Sustainable and Circular Textiles*. [PDF file]. URL: https://ec.europa.eu/environment/circular-economy/pdf/textiles-strategy.pdf.

Freire, C.S.R. et al. (2006). 'Controlled heterogeneous modification of cellulose fibers with fatty acids: Effect of reaction conditions on the extent of esterification and fiber properties'. In: *Journal of Applied Polymer Science* 100.2, pp. 1093–1102. DOI: https://doi.org/10.1002/app.23454. eprint: https://onlinelibrary.wiley.com/doi/pdf/10.1002/app.23454. URL: https://onlinelibrary.wiley.com/doi/abs/10.1002/app.23454.

Friebolin, H. (2011). *Basic one-and two-dimensional NMR spectroscopy*. 5th. Wiley-VCH.

Gao, C., Liu, S. and Edgar, K.J. (2018). 'Regioselective chlorination of cellulose esters by methanesulfonyl chloride'. In: *Carbohydrate Polymers* 193, pp. 108–118. ISSN: 0144-8617. DOI: https://doi.org/10.1016/j.carbpol.2018.03.093. URL: https://www.sciencedirect.com/science/article/pii/S0144861718303576.

Gericke, M. et al. (2012). 'Studies on the tosylation of cellulose in mixtures of ionic liquids and a co-solvent'. In: *Carbohydrate Polymers* 89.2, pp. 526–536. ISSN: 0144-8617. DOI: https://doi.org/10.1016/j.carbpol.2012.03.040. URL: https://www.sciencedirect.com/science/article/pii/S0144861712002536.

Granström, M. et al. (2008). 'Tosylation and acylation of cellulose in 1-allyl-3-methylimidazolium chloride'. In: *Cellulose* 15, pp. 481–488.

Hassan, E-S.R.E. et al. (2013). 'Studies on the Dissolution of Glucose in Ionic Liquids and Extraction Using the Antisolvent Method'. In: *Environmental Science & Technology* 47.6. PMID: 23398175, pp. 2809–2816. DOI: 10.1021/es303884n. eprint: https://doi.org/10.1021/es303884n. URL: https://doi.org/10.1021/es303884n.

Heinze, T., Liebert, T. and Koschella, A. (2006). *Esterification of Polysaccharides*. Springer Laboratory. Springer Berlin Heidelberg. ISBN: 978-3-540-32112-5. URL: https://books.google.no/books?id=HMlNKY8e1FsC.

Hellesnes, K.N. et al. (2023). 'Biochemical Characterization and NMR Study of a PET-Hydrolyzing Cutinase from Fusarium solani pisi'. In: *Biochemistry* 62.8. PMID: 36967526, pp. 1369–1375. DOI: 10.1021/acs.biochem.2c00619. eprint: https://doi.org/10.1021/acs.biochem.2c00619. URL: https://doi.org/10.1021/acs.biochem.2c00619.

Ilyas, M. et al. (2018). 'Plastic waste as a significant threat to environment – a systematic literature review'. In: *Reviews on Environmental Health* 33.4, pp. 383–406. DOI: doi:10.1515/reveh-2017-0035. URL: https://doi.org/10.1515/reveh-2017-0035.

Jones, S.T. et al. (2020). 'Modified cyclodextrins as broad-spectrum antivirals'. In: *Science Advances* 6.5, eaax9318. DOI: 10.1126/sciadv.aax9318. eprint: https://www.science.org/doi/pdf/10.1126/sciadv.aax9318. URL: https://www.science.org/doi/abs/10.1126/sciadv.aax9318.

Kari, J. et al. (2019). 'A practical approach to steady-state kinetic analysis of cellulases acting on their natural insoluble substrate'. In: *Analytical Biochemistry* 586, p. 113411. ISSN: 0003-2697. DOI: https://doi.org/10.1016/j.ab.2019.113411. URL: https://www.sciencedirect.com/science/article/pii/S0003269719306694.

Koschella, A. and Heinze, T. (2003). 'Unconventional cellulose products by fluorination of tosyl cellulose'. In: *Macromolecular Symposia* 197.1, pp. 243–254. DOI: https://doi.org/10.1002/masy.200350722. eprint: https://onlinelibrary.wiley.com/doi/pdf/10.1002/masy.200350722. URL: https://onlinelibrary.wiley.com/doi/abs/10.1002/masy.200350722.

Lease, J., Kawano, T. and Andou, Y. (2021). 'Esterification of Cellulose with Long Fatty Acid Chain through Mechanochemical Method'. In: *Polymers* 13.24. ISSN: 2073-4360. DOI: 10.3390/polym13244397. URL: https://www.mdpi.com/2073-4360/13/24/4397.

Li, W.C., Tse, H.F. and Fok, L. (2016). 'Plastic waste in the marine environment: A review of sources, occurrence and effects'. In: *Science of The Total Environment* 566-567, pp. 333–349. ISSN: 0048-9697. DOI: https://doi.org/10.1016/j.scitotenv.2016.05.084. URL: https://www.sciencedirect.com/science/article/pii/S0048969716310154.

Long, T.E. and Scheirs, J. (2005). *Modern polyesters: chemistry and technology of polyesters and copolyesters*. John Wiley & Sons.

López, M.d.M.C. et al. (2014). 'Assessing changes on poly(ethylene terephthalate) properties after recycling: Mechanical recycling in laboratory versus postconsumer recycled material'. In: *Materials Chemistry and Physics* 147.3, pp. 884–894. ISSN: 0254-0584. DOI: https://doi.org/10.1016/j.matchemphys.2014.06.034. URL: https://www.sciencedirect.com/science/article/pii/S025405841400385X.

Matuszek, K. et al. (2020). 'Studies on the Solubility of Terephthalic Acid in Ionic Liquids'. In: *Molecules* 25.1. ISSN: 1420-3049. DOI: 10.3390/molecules25010080. URL: https://www.mdpi.com/1420-3049/25/1/80.

Melton, L.D. and Slessor, K.N. (1971). 'Synthesis of monosubstituted cyclohexaamyloses'. In: *Carbohydrate Research* 18.1, pp. 29–37. ISSN: 0008-6215. DOI: https://doi.org/10.1016/S0008-6215(00)80256-6. URL: https://www.sciencedirect.com/science/article/pii/S0008621500802566.

Mocanu, G., Constantin, M. and Carpov, A. (1996). 'Chemical reactions on polysaccharides, 5. Reaction of mesyl chloride with pullulan'. In: *Die Angewandte Makromolekulare Chemie: Applied Macromolecular Chemistry and Physics* 241.1, pp. 1–10.

Murai, S. et al. (1998). 'Removal of phthalic acid esters from aqueous solution by inclusion and adsorption on β-cyclodextrin'. In: *Environmental science & technology* 32.6, pp. 782–787.

Piribauer, B. and Bartl, A. (2019). 'Textile recycling processes, state of the art and current developments: A mini review'. In: *Waste Management & Research* 37.2. PMID: 30632932, pp. 112–119. DOI: 10.1177/0734242X18819277. eprint: https://doi.org/10.1177/0734242X18819277. URL: https://doi.org/10.1177/0734242X18819277.

Pirillo, V., Pollegioni, L. and Molla, G. (2021). 'Analytical methods for the investigation of enzyme-catalyzed degradation of polyethylene terephthalate'. In: *The FEBS Journal* 288.16, pp. 4730–4745.

Pretsch, E. et al. (2013). *Tables of spectral data for structure determination of organic compounds*. Springer Science & Business Media.

Rathod, R.H. et al. (2019). 'Ultra-high performance liquid chromatography-MS/MS (UHPLC-MS/MS) in practice: Analysis of drugs and pharmaceutical formulations'. In: *Future Journal of Pharmaceutical Sciences* 5.1, pp. 1–26.

Schneider, H-J. et al. (1998). 'NMR Studies of Cyclodextrins and Cyclodextrin Complexes'. In: *Chemical Reviews* 98.5. PMID: 11848948, pp. 1755–1786. DOI: 10.1021/cr970019t. eprint: https://doi.org/10.1021/cr970019t. URL: https://doi.org/10.1021/cr970019t.

Shojaei, B., Abtahi, M. and Najafi, M. (2020). 'Chemical recycling of PET: A stepping-stone toward sustainability'. In: *Polymers for Advanced Technologies* 31.12, pp. 2912–2938. DOI: https://doi.org/10.1002/pat.5023. eprint: https://onlinelibrary.wiley.com/doi/pdf/10.1002/pat.5023. URL: https://onlinelibrary.wiley.com/doi/abs/10.1002/pat.5023.

Silverstein, R.M. et al. (2014). *Spectrometric identification of organic compounds*. 8th. Wiley Global Education.

Solomons, T.W.G. and Fryhle, C.B. (2007). *Organic chemistry*. 9th. John Wiley & Sons.

Steed, J.W. and Atwood, J.L. (2000). *Supramolecular Chemistry*. Wiley. ISBN: 978-0-471-98791-8. URL: https://books.google.no/books?id=1IgvAQAAIAAJ.

Takada, A. and Kadokawa, J. (2022). 'Preparation of cellulosic soft and composite materials using ionic liquid media and ion gels'. In: *Cellulose* 29.5, pp. 2745–2754.

Tan, D. and Friščić, T. (2018). 'Mechanochemistry for Organic Chemists: An Update'. In: *European Journal of Organic Chemistry* 2018.1, pp. 18–33. DOI: https://doi.org/10.1002/ejoc.201700961. eprint: https://chemistry-europe.onlinelibrary.wiley.com/doi/pdf/10.1002/ejoc.201700961. URL: https://chemistry-europe.onlinelibrary.wiley.com/doi/abs/10.1002/ejoc.201700961.

Thiounn, T. and Smith, R.C. (2020). 'Advances and approaches for chemical recycling of plastic waste'. In: *Journal of Polymer Science* 58.10, pp. 1347–1364. DOI: https://doi.org/10.1002/pol.20190261. eprint: https://onlinelibrary.wiley.com/doi/pdf/10.1002/pol.20190261. URL: https://onlinelibrary.wiley.com/doi/abs/10.1002/pol.20190261.

Thomsen, T.B. et al. (2023). 'A new continuous assay for quantitative assessment of enzymatic degradation of poly(ethylene terephthalate) (PET)'. In: *Enzyme and Microbial Technology* 162, p. 110142. ISSN: 0141-0229. DOI: https://doi.org/10.1016/j.enzmictec.2022.110142. URL: https://www.sciencedirect.com/science/article/pii/S0141022922001612.

Tournier, V. et al. (Apr. 2020). 'An engineered PET depolymerase to break down and recycle plastic bottles'. In: *Nature* 580.7802, pp. 216–219. ISSN: 0028-0836. DOI: 10.1038/s41586-020-2149-4. URL: https://doi.org/10.1038/s41586-020-2149-4.

Vollmer, I. et al. (2020). 'Beyond Mechanical Recycling: Giving New Life to Plastic Waste'. In: *Angewandte Chemie International Edition* 59.36, pp. 15402–15423. DOI: https://doi.org/10.1002/anie.201915651. eprint: https://onlinelibrary.wiley.com/doi/pdf/10.1002/anie.201915651. URL: https://onlinelibrary.wiley.com/doi/abs/10.1002/anie.201915651.

Wei, R. et al. (2020). 'Possibilities and limitations of biotechnological plastic degradation and recycling'. In: *Nature Catalysis* 3, pp. 867–871.

Wu, H. et al. (2022). 'Rapid construction of cyclodextrin polyester layer on polyamide for preparing highly permeable reverse osmosis membrane'. In: *Journal of Membrane Science* 660, p. 120862. ISSN: 0376-7388. DOI: https://doi.org/10.1016/j.memsci.2022.120862. URL: https://www.sciencedirect.com/science/article/pii/S037673882200607X.

Xu, D. et al. (2011). 'Studies on regioselective acylation of cellulose with bulky acid chlorides'. In: *Cellulose* 18, pp. 405–419.

Yang, Y. et al. (2021). 'Recent Progress on Cellulose-Based Ionic Compounds for Biomaterials'. In: *Advanced Materials* 33.28, p. 2000717. DOI: https://doi.org/10.1002/adma.202000717. eprint: https://onlinelibrary.wiley.com/doi/pdf/10.1002/adma.202000717. URL: https://onlinelibrary.wiley.com/doi/abs/10.1002/adma.202000717.

Yoshida, S. et al. (2016). 'A bacterium that degrades and assimilates poly(ethylene terephthalate)'. In: *Science* 351.6278, pp. 1196–1199. DOI: 10.1126/science.aad6359. eprint: https://www.science.org/doi/pdf/10.1126/science.aad635. URL: https://www.science.org/doi/abs/10.1126/science.aad6359.

Zweckmair, T. et al. (2015). 'On the mechanism of the unwanted acetylation of polysaccharides by 1, 3-dialkylimidazolium acetate ionic liquids: Part 1—Analysis, acetylating agent, influence of water, and mechanistic considerations'. In: *Cellulose* 22, pp. 3583–3596.

A Additional results for Reaction 1

HMBC correlations between pyridine signals and glucose signals (Figure A.1), along with HSQC spectrum (Figure A.2) of the product from Reaction 1 (Table 3) distinguish compounds i, ii, iii, iv, v, and vi.

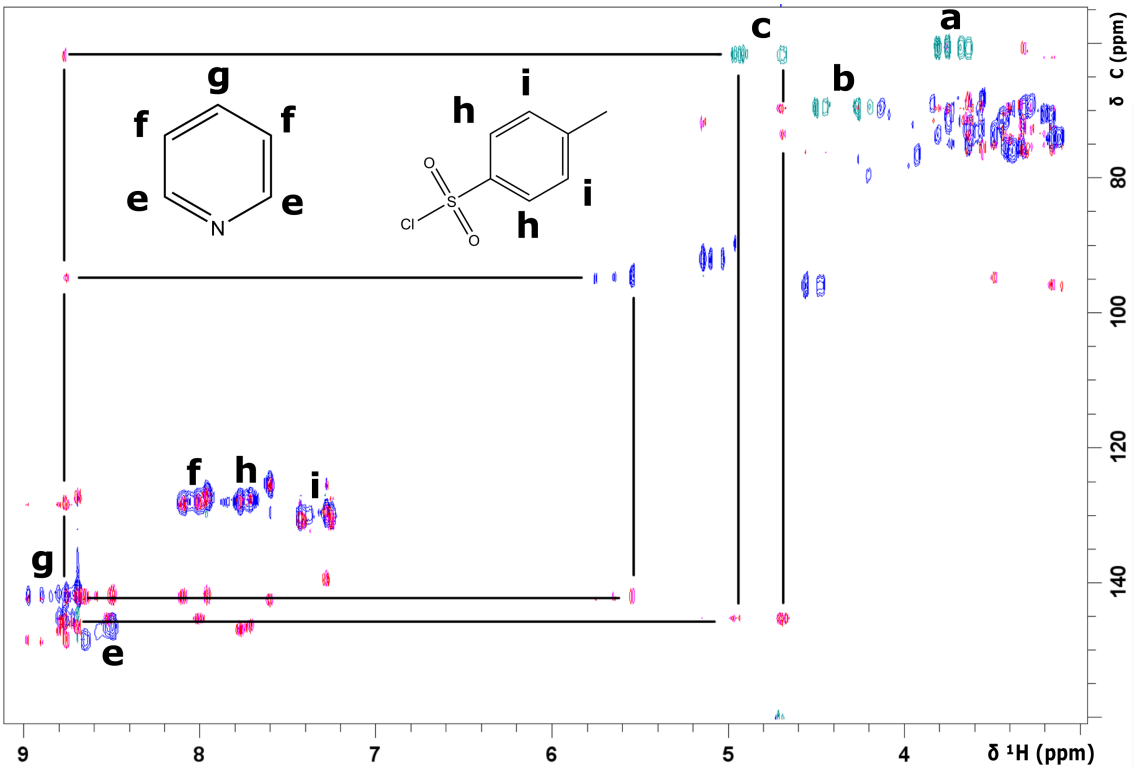

Figure A.1: HSQC-spectrum overlaid HMBC spectrum of product from Reaction 1 (Table 3), dissolved in D_2O. Blue signals are CH- and CH_3-protons, while green signals are CH_2-protons, red signals are HMBC correlations. Chemical shifts for glucose H6 (a (3.7 ppm, 61 ppm), b (4.35 ppm, 69.5 ppm), and c (4.8 ppm, 62 ppm)), pyridine (e (8.5 ppm, 147 ppm), f (8 ppm, 128 ppm), g (8.7 ppm, 142 ppm)), and tosyl groups (h (7.7 ppm, 126 ppm), i (7.3 ppm, 130 ppm) were assigned. HMBC correlations between signals e or g and c are shown, as well as HMBC correlation between g and perhaps an anomeric proton (unassigned, (5.55 ppm, 95 ppm). Recorded at 298 K.

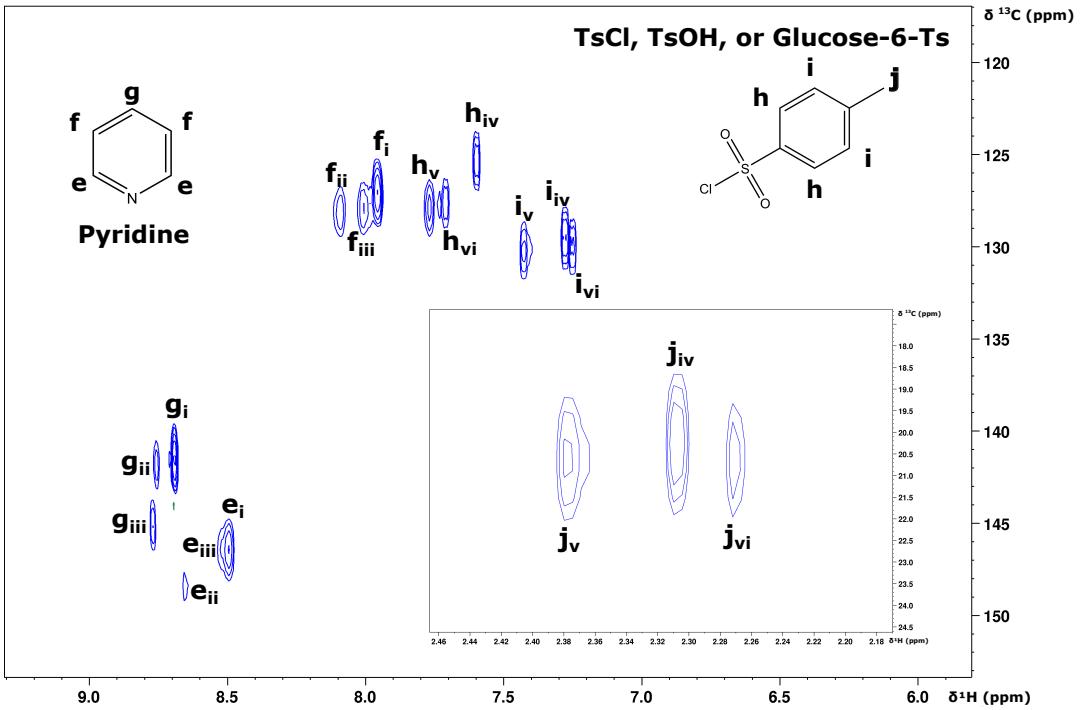

Figure A.2: Regions of HSQC spectrum from the product of Reaction 1 (Table 3). Pyridine and tosyl protons were given letters e, f, g, h, i, and j. Annotated peaks distinguish three different pyridines, annotated i, ii, and iii, and three different tosyl groups, annotated iv, v, vi. The different tosyl groups were distinguished by HMBC, but not assigned further. Pyridine: e_i (8.49 ppm, 146 ppm), f_i (7.96 ppm, 127), g_i (8.69 ppm, 141 ppm). Pyridine with HMBC correlation to glucose C1: e_{ii} (8.66 ppm, 148 ppm), f_{ii} (8.09 ppm, 128 ppm), g_{ii} (8.76 ppm, 142 ppm). Pyridine with HMBC correlation to glucose C6: e_{iii} (8.52 ppm, 146 ppm), f_{iii} (8.01 ppm, 128 ppm), g_{iii} (8.77 ppm, 145 ppm). Ts_{iv}: h_{iv} (7.59 ppm, 125 ppm), i_{iv} (7.29 ppm, 129 ppm), j_iv (2.31 ppm, 20 ppm). Ts_v: h_v (7.77 ppm, 128 ppm), i_v (7.43 ppm, 130 ppm), j_v (2.38 ppm, 21 ppm). Ts_{vi}: h_{vi} (7.70 ppm, 128 ppm), i_{vi} (7.25 ppm, 130 ppm), j_vi (2.27 ppm, 21 ppm). Recorded at 298 K with D_2O as solvent.

B Additional results for Reaction 2

Regions of the HSQC spectrum from the terephthalation of glucose in pyridine (Reaction 2 in Table 3) is shown in Figure B.1.

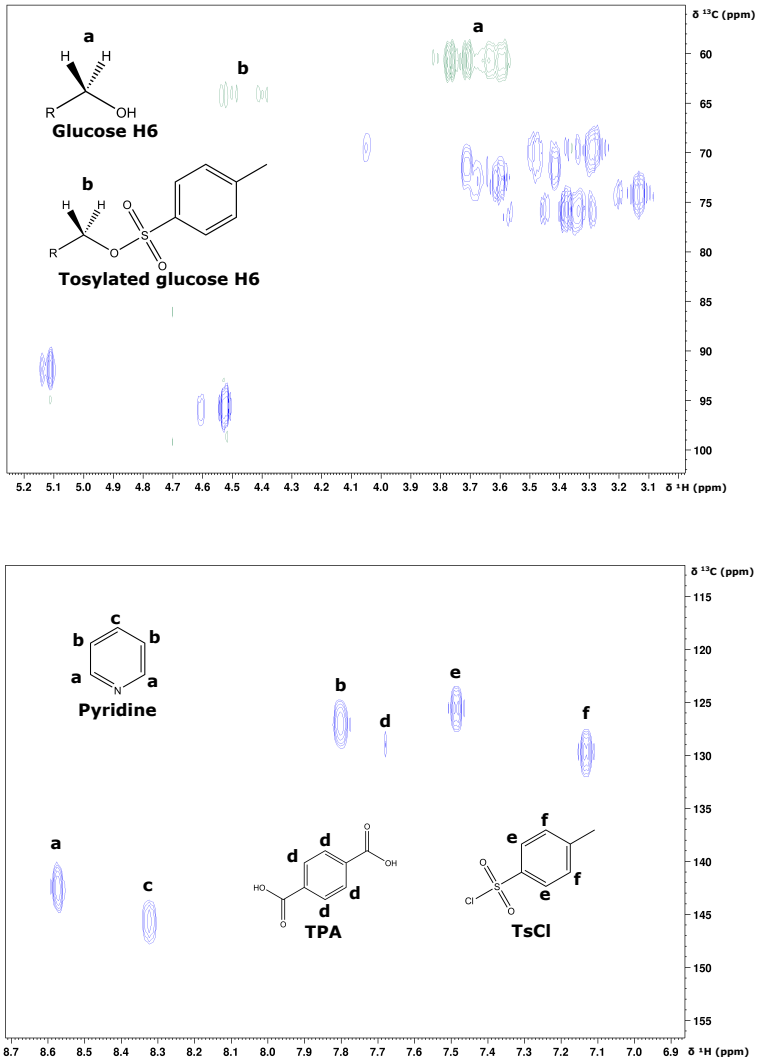

Figure B.1: Regions of HSQC spectrum from the product of terephthalation of glucose in pyridine dissolved in D_2O. Top: Glucose signals showing different glucose CH_2-signals labelled a (3.7 ppm, 61 ppm), b (4.46 ppm, 64 ppm). Bottom: Aromatic region with signals for pyridine (a (8.6 ppm, 142 ppm), b (7.8 ppm, 127 ppm), c (8.3 ppm, 146 ppm)) TPA signal d (7.7 ppm, 129 ppm), and tosyl protons (e (7.5 ppm, 126 ppm), f (7.1 ppm, 130 ppm). Recorded at 298 K.

C Additional results for Reaction 3

A part of the HSQC spectrum from the liquid fraction from water precipitation of the BMIMCl-phase in the terephthalation of glucose in BMIMCl (Reaction 3 in Table 3) is shown in Figure C.1.

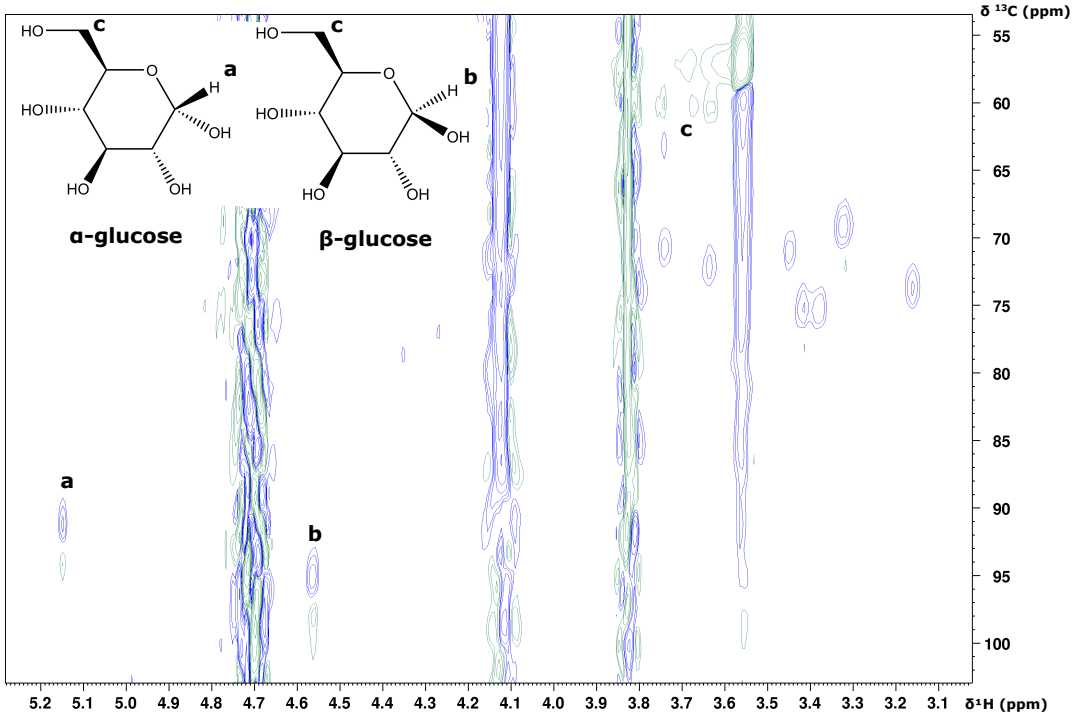

Figure C.1: Part of HSQC spectrum from the water fraction obtained after water precipitation of the BMIMCl-phase for the terephthalation of glucose in BMIMCl. CH- and CH_3-hydrogens give blue signals, while CH_2-hydrogens give green signals. Two anomeric proton signals were annotated for α-glucose a (5.15 ppm, 90 ppm) and β-glucose b (4.6 ppm, 95 ppm), as well as glucose H6 signal c (3.7 ppm, 60 ppm). Recorded at 298 K in 10% D_2O.

D Additional results for Reaction 4

Sugar- and aromatic regions of the HSQC spectrum of the precipitated fraction (dissolved in DMSO-d_6-d_6-d_6) from the terephthalation of cellopentaose (Reaction 4 in Table 3 are shown in Figure D.1

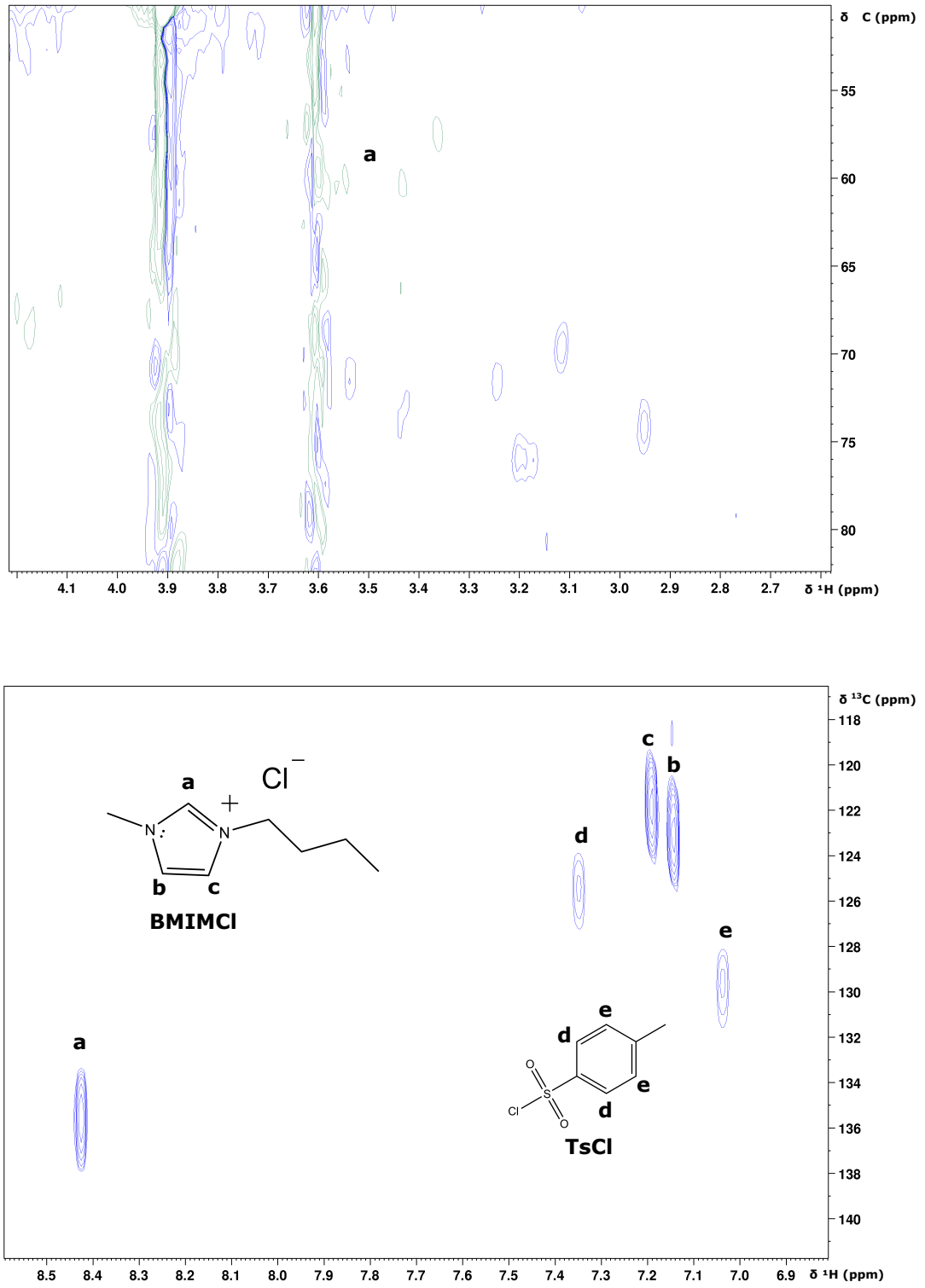

Figure D.1: Regions of HSQC spectrum of the water precipitate dissolved in DMSO-d_6-d_6-d_6 from terephthalation of cellopentaose. Top: Sugar signal region. Weak CH_2 signal a (3.5 ppm, 60.5 ppm) assigned as H6 of cellopentaose. Includes unassigned signals assumed to originate from cellopentaose. Bottom: Aromatic region, showing signals for BMIMCl (a (8.42 ppm, 136 ppm), b (7.14 ppm, 123 ppm), c (7.19 ppm, 122 ppm)) and TsCl (d (7.35 ppm, 126 ppm), e (7.04 ppm, 130 ppm)), and absence of TPA signal. Recorded at 298 K.

E FTIR spectra for Reaction 5

FTIR spectra for the tosylation (Top) and terephthalation (Bottom) of cellulose (Reaction 5 in Table 3) are given in Figure E.1. All annotated bands from the figure are given here, but all are not assigned. Assignments are found in the figure text of Figure E.1.

TOSC FTIR cm^{-1}: 3340, 3110, 2961, 2933, 2875, 1635, 1571, 1444, 1371, 1335, 1315, 1163, 1109, 1057, 1033, 1011, 753, 682, 652, 620, 567.

Terephthalated cellulose FTIR cm^{-1}: 3336, 3062, 2872, 2654, 2523, 2114, 1671, 1572, 1509, 1422, 1278, 1161, 1134, 1110, 1055, 1032, 1017, 927, 878, 780, 726, 666, 617, 558, 524, 446.

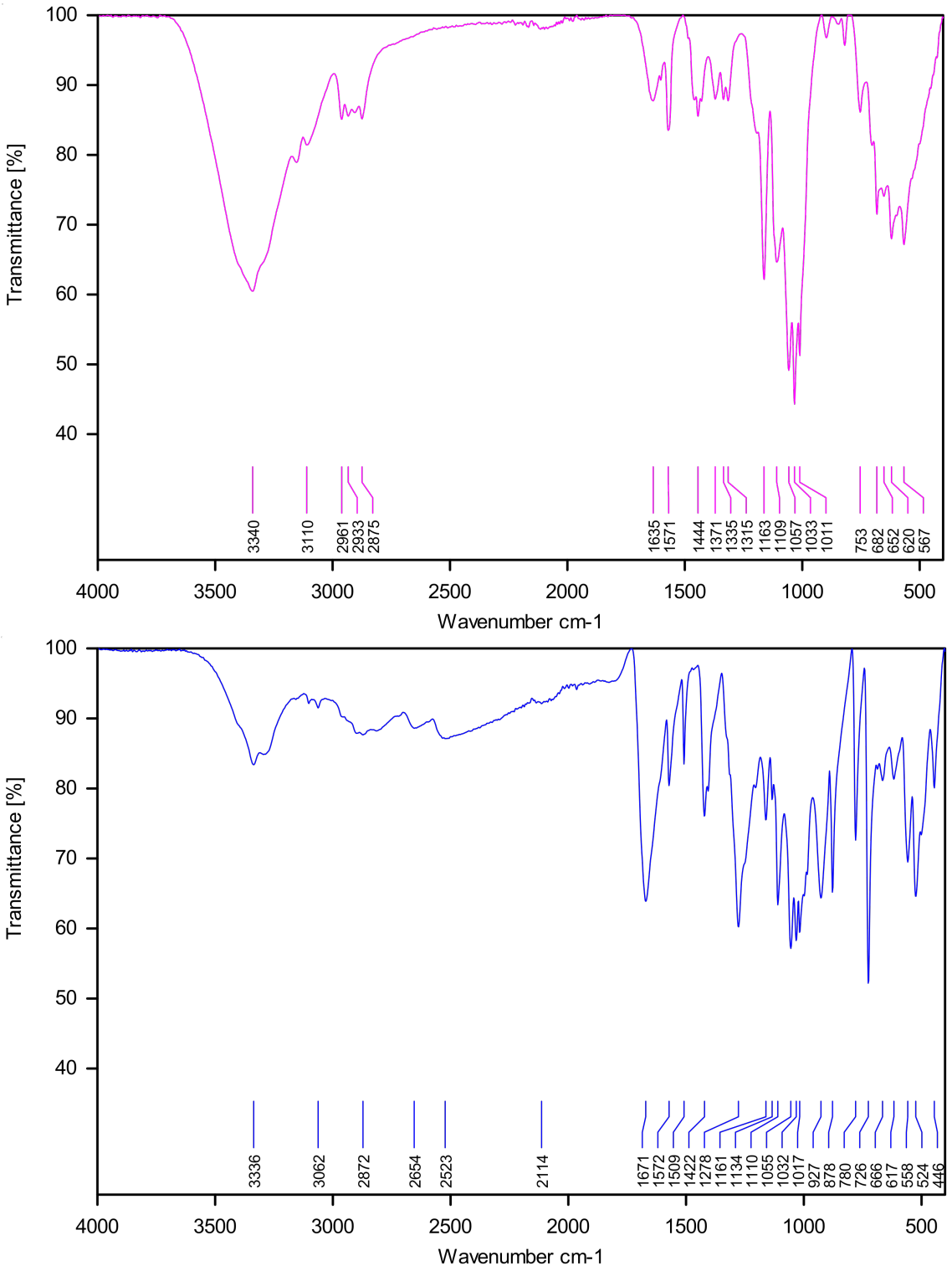

Figure E.1: FTIR spectra of products from tosylation of cellulose (top) and terephthalation of tosylated cellulose (bottom). Tosylated cellulose, FTIR (cm^{-1}): 3340 (OH stretch), 2875 (CH_2 symmetric stretch), 1635 (Adsorbed water), 1571 (Aromatic ring stretch), 1163 (C-O-C antisymmetric stretch), 1109 (Pyranose ring antisymmetric stretch), 1057 (C-O stretch), 1033 (C-O stretch), 1011 (C-O stretch). Terephthalated cellulose, FTIR (cm^{-1}): 3336 (OH stretch), 2872 (CH_2 symmetric stretch), 1671 (C=O stretch of TPA), 1572 (Aromatic ring stretch), 1161 (C-O-C antisymmetric stretch), 1110 (Pyranose ring antisymmetric stretch), 1055 (C-O stretch), 1032 (C-O stretch), 1017 (C-O stretch).

F Additional results for Reaction 6

The HSQC spectrum for the syrup-like product from the tosylation of β-CD (Reaction 6 in Table 3) is shown in Figure F.1.

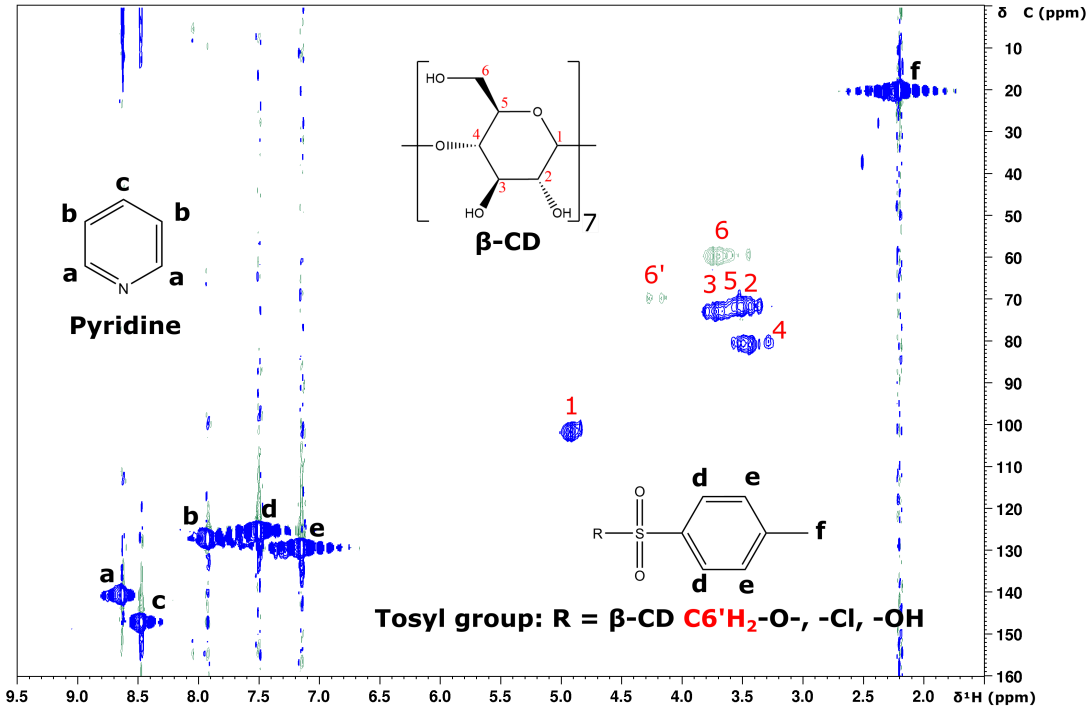

Figure F.1: HSQC spectrum of the product from tosylation of β-CD, dissolved in D_2O. Signals pyridine (a (8.6 ppm, 141 ppm), b (7.9 ppm, 127 ppm), c (8.5 ppm, 147 ppm)) and tosyl group (d (7.5 ppm, 125 ppm), e (7.1 ppm, 130 ppm), f (2.2 ppm, 20 ppm)) are marked. β-CD protons are numbered as given in Figure 5, with 6' (4.2 ppm, 70 ppm) being tosylated β-CD H6. Recorded at 298 K.

G Diffusion coefficients for Reaction 7

Diffusion coefficients reported by selected protons from DOSY performed on the product of NaOH-activated terephthalation of β-CD dissolved in D_2O (Reaction 7 in Table 3) are shown in Table G.1.

Table G.1: Estimated diffusion coefficients for selected protons of β-CD, tosyl moieties, TPA, and pyridine in the precipitated product of NaOH-activated terephthalation of β-CD dissolved in DMSO-d_6-d_6-d_6, obtained using DOSY at 298K.

Assignment	δ^1**H [ppm]**	δ^{13}**C [ppm]**	**Diffusion coefficient** [$\times 10^{-11}$ m^2/s]
β-CD H1	4.79	102	0.1
β-CD H1	4.85	102	1.1
β-CD H2	3.21	72	2.2
β-CD H3	3.58	73	2.5
β-CD H4	3.45	81	2.8
β-CD H4	3.39	82	2.1
β-CD H4	3.25	82	2.1
β-CD H6	3.64	60	2.3
β-CD H6	3.46	60	2.7
β-CD H6'	4.33	70	2.4
β-CD H6'	4.19	70	2.4
Ts-CH_3'	2.39	21.5	2.4
Ts-Ar'	7.41	130	2.9
Ts-Ar'	7.73	128	2.1
TPA	8.04	130	4.2
Ts-CH_3	2.28	21	5.7
Ts-Ar	7.12	129	6.7
Ts-Ar	7.50	126	8.3
Pyridine	7.85	138	10
Pyridine	7.44	125	11
Pyridine	8.60	149	15

H Raw data for section 4.2

H.1 Raw data for CD:TPA inclusion complex experiments

Raw data from the titration experiments (See section 3.4) for the CD:TPA inclusion complex, taken from HSQC spectra, is shown in tables H.1 and H.2, for β-CD and α-CD, respectively.

Table H.1: Chemical shift changes for β-CD protons, recorded at constant concentration of β-CD 1.5 mM and different concentrations of TPA, measured by euclidean distance from control β-CD proton signals (1.5 mM β-CD) and 0 mM TPA.

	$\Delta\delta^1$**H [ppm]**					
[TPA] [mM]	**H1**	**H2**	**H3**	**H4**	**H5**	**H6**
0	0	0	0	0	0	0
0.58	0	0	0	0.0054	0.003	0
1.30	0.0002	0.0026	0.0052	0.0052	0.013	0.0001
1.74	0	0.0054	0.0053	0.0054	0.016	0
2.61	0.0053	0.0054	0.011	0.011	0.024	0
3.77	0.0052	0.011	0.011	0.011	0.029	0.005
5.79	0.011	0.016	0.016	0.016	0.040	0.008
21.1	0.032	0.043	0.064	0.038	0.13	0.030

Table H.2: Chemical shift changes for α-CD protons, recorded at constant concentration of α-CD 1.5 mM and different concentrations of TPA, measured by euclidean distance from control α-CD proton signals (1.5 mM α-CD) and 0 mM TPA.

	$\Delta\delta^1$**H [ppm]**					
[TPA] [mM]	**H1**	**H2**	**H3**	**H4**	**H5**	**H6**
0.00	0	0	0	0	0	0
0.57	0.0010	0.0012	0.002	0.00093	0.0054	0
1.29	0.0021	0.0019	0.0045	0.0018	0.0088	0.0007
1.72	0.0024	0.0026	0.0058	0.0022	0.0080	0
2.58	0.0031	0.0037	0.0088	0.0031	0.012	0.0017
3.73	0.0039	0.0049	0.012	0.0037	0.017	0.0007
5.74	0.0060	0.0078	0.019	0.0058	0.024	0.0027
7.93	0.0091	0.012	0.031	0.0085	0.033	0.0019

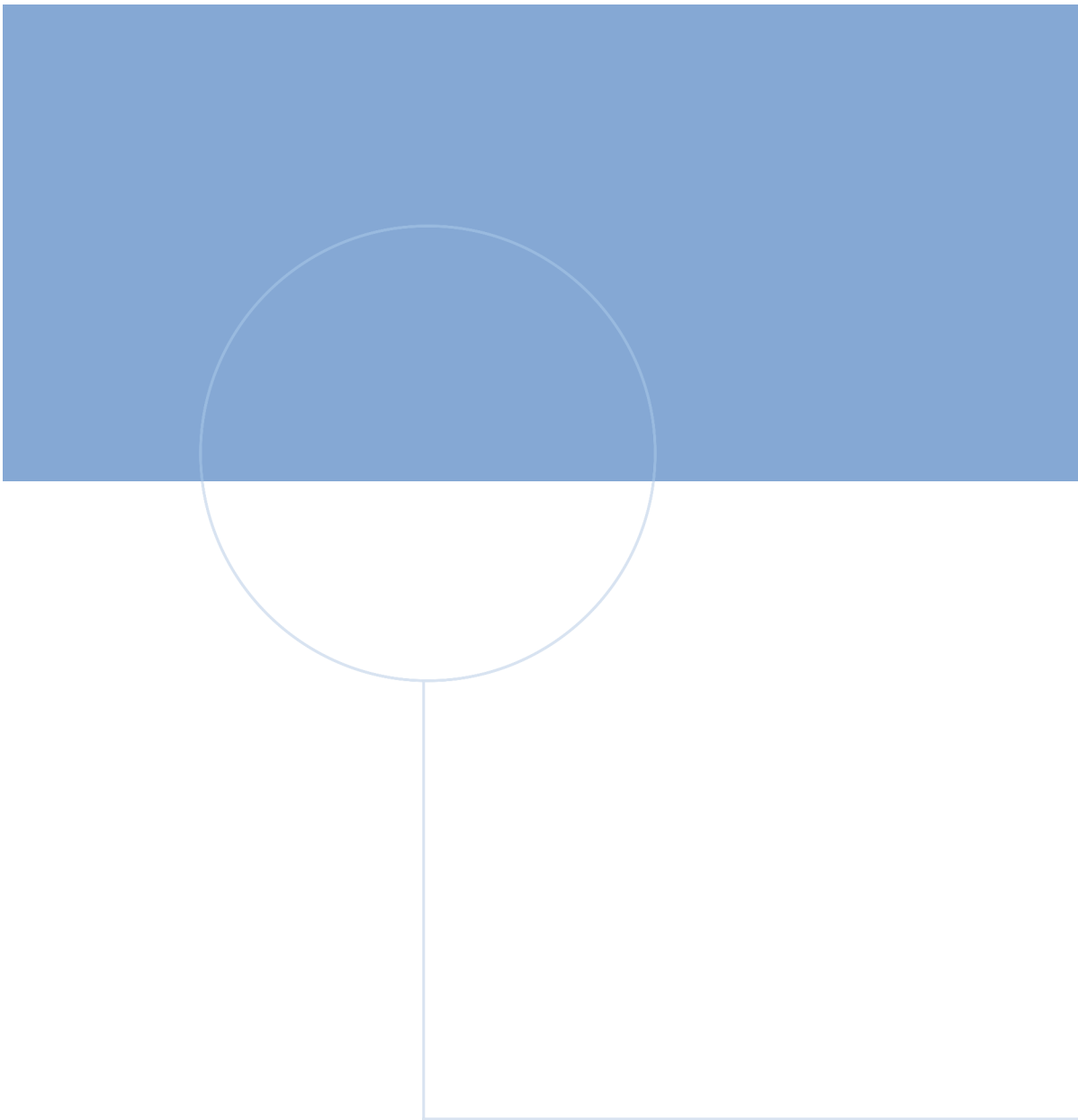

NTNU

Norwegian University of
Science and Technology